REPORT DOCUMENTATION PAGE

Form Approved
OMB No. 0704-0188

1. AGENCY USE ONLY *(Leave blank)*

2. REPORT DATE Dec 94

3. REPORT TYPE AND DATES COVERED

4. TITLE AND SUBTITLE
A nonintrusive method of Quantifying flow Visualization Data in Vortex Flow Fields

5. FUNDING NUMBERS

6. AUTHOR(S)
Vincent Joseph Sci

7. PERFORMING ORGANIZATION NAME(S) AND ADDRESS(ES)
AFIT Students Attending:

Texas A & M

8. PERFORMING ORGANIZATION REPORT NUMBER
AFIT/CI/CIA

94-170

9. SPONSORING/MONITORING AGENCY NAME(S) AND ADDRESS(ES)
DEPARTNEMT OF THE AIR FORCE
AFIT/CI
2950 P STREET, BDLG 125
WRIGHT-PATTERSON AFB OH 45433-7765

10. SPONSORING/MONITORING AGENCY REPORT NUMBER

11. SUPPLEMENTARY NOTES

12a. DISTRIBUTION/AVAILABILITY STATEMENT
Approved for Public Release IAW AFR 190-1
Distribution Unlimited
BRIAN D. GAUTHIER, MSgt, USAF
Chief Administration

12b. DISTRIBUTION CODE

13. ABSTRACT *(Maximum 200 words)*

14. SUBJECT TERMS

15. NUMBER OF PAGES 73

16. PRICE CODE

17. SECURITY CLASSIFICATION OF REPORT	18. SECURITY CLASSIFICATION OF THIS PAGE	19. SECURITY CLASSIFICATION OF ABSTRACT	20. LIMITATION OF ABSTRACT

94-170

A NONINTRUSIVE METHOD OF QUANTIFYING FLOW VISUALIZATION DATA IN VORTEX FLOW FIELDS

A Thesis

by

VINCENT JOSEPH SEI

Submitted to the Office of Graduate Studies of
Texas A&M University
in partial fulfillment of the requirements for the degree of

MASTER OF SCIENCE

December 1994

Major Subject: Aerospace Engineering

ABSTRACT

A Nonintrusive Method of Quantifying Flow Visualization Data in Vortex Flow Fields.

(December 1994)

Vincent Joseph Sei, B.S. United States Air Force Academy

Chair of Advisory Committee: Dr. Donald T. Ward

The High Angle of Attack Research Vehicle (HARV) as well as other similar flight test aircraft have been using smoke flow visualization techniques to characterize the vortex flow created by leading edge extensions and the forebody. With the advent of video measurement techniques, this type of flow visualization can not only provide a qualitative assessment of the flow but also a quantitative measure to be used to validate computational fluid dynamic codes and wind tunnel test.

One of the major drawbacks to employing video imaging was the introduction of false motion due to camera movement in flight. A relative motion approach using fixed targets along with the flow visualization scheme was utilized to remove unwanted motion. The relative motion algorithm was tested using a laboratory test setup where cameras underwent both translational and rotational motion to simulate both wing bending and torsion. The method was effective in removing both motions with only a slight loss of accuracy.

A full scale mockup of the HARV demonstrated that the location of a target could be determined within one inch of its true position or less than 1% of the HARV length .

DEDICATION

This thesis is dedicated to all those who have made the ultimate sacrifice in the defense of this great country. May God bless and keep them. It is also dedicated to all Snoopy Troopers, past, present and future. God's Speed.

ACKNOWLEDGMENTS

I would like to thank all of the people who gave of themselves to aid in the success of this effort. Dr. Donald Ward not only served as my graduate advisor, but went out of his way to bring more airplane examples into the classroom. He always brought with him patience, dedication and insight. This project would not have gone as far without him. I would also like to acknowledge Dr. Strganac, and Dr. Painter for taking time out of the busy schedules to serve on my committee. Todd Oneil deserves special thanks for allowing me to borrow his wind tunnel platform for my experiment. Not only was he generous to lend me the equipment, but was gracious enough to help me repair it both times I broke it. Finally, to Judy Blanchard who generously provided me with an endless supply of rubber bands for the test board.

As with allot of projects, this could not have come about without the financial support of the Fannie and John Hertz Foundation which covered by tuition in graduate school.

Thanks also go to my mother and father, Helen and Richard Sei, for the endless amount of love and guidance they have provided me through the years. To Sarah Daniels, and Bill "Knux" White, who have always managed to believe in me through the years. The last note of thanks goes to the Good Lord who has never failed to see me through the tough times.

TABLE OF CONTENTS

Page

TABLE OF CONTENTS (CONTINUED)

Page

LIST OF TABLES

Page

LIST OF FIGURES

Page

LIST OF FIGURES (CONTINUED)

Page

LIST OF FIGURES (CONTINUED)

Page

NOMENCLATURE

AOA	Angle of Attack
CFD	Computational Fluid Dynamics
CALI	Camera position calibration subroutine for EV
EV	ExpertVision
FVC	Forebody Vortex Control
HARV	High Angle Of Attack Research Vehicle
HATP	High Alpha Technology Program
LEX	Leading Edge Extension
MATV	Multi Axis Thrust Vectoring
NASA	National Aeronautics and Space Administration
TRAC	Trajectory calculation subroutine for EV
TRED	Trajectory editor for EV
VAC	Video Analog Collection
α	Angle of Attack

INTRODUCTION

Currently the National Aeronautics and Space Administration (NASA), is researching the dynamic flow characteristics of fighters in High Angle of Attack flight regimes. One of the major thrusts of the program is to quantitatively measure vortical flow over NASA's F/A-18 High Angle of Attack Research Vehicle (HARV). With this information, better computational fluid dynamic codes (CFD), and methods of controlling vortical flow will be developed to enhance pre and post stall maneuvering of future fighter aircraft.

A significant problem arises in being able to determine the trajectory as well as the velocity of a vortex produced by a leading edge extension (LEX) during actual test flights. Conventional methods from the wind tunnel, pitot static probes and laser light sheets, do not lend themselves readily to actual flight test because of weight, power, time, and cost considerations. This problem, however, lends itself to using video data obtained in-flight to determine quantitative vortical flow data. The thrust of this research is to develop a method which will use in flight video to calculate the position and velocity of a vortex during both steady state and dynamic maneuvering.

Background

The latest generations of fighter aircraft, like the F-16, and F/A-18, rely heavily upon the use of vortex lift to enhance maneuverability, and high angle of attack capabilities. Unexpected control problems encountered during the flight test programs of these two aircraft demonstrate that there is a need for improving high angle of attack prediction capabilities. A deep stall phenomena was encountered in

---

This thesis follows the style and format of the *AIAA Journal of Aircraft.*

the F-16 which required the enlargement of the horizontal tail, while the F/A-18 experienced lateral/directional shortcomings which were corrected with improvements to the control laws.[1] The F/A-18 also went on to experience problems in its operational career with fatigue in the vertical stabilizers due to unexpected side loads produced by the breakdown of the vortex shed by the LEX.[1] These problems, along with the desire to utilize thrust vectoring and forebody vortex control as a means of post stall maneuvering in the next generation of fighters, NASA initiated the High Alpha Technology Program (HATP) to develop the necessary knowledge base.

The objectives of the HATP program include (1) detailing Reynolds and Mach number effects, (2) increasing the understanding of vortical flow about a vehicle, (3) determining if there was a systematic problem that led to poor prediction with the F/A-18, and (4) correlation between tunnel, CFD, and flight test.[1]

As stated previously, one of the major priorities of the NASA High Alpha Technology Program is to correlate results of CFD, along with wind tunnel results, to those obtained with the actual HARV vehicle in flight (Fig. 1).[1-6] The flight results, however, have mainly been qualitative with the use of smoke flow visualization, tufts, and surface dye.[7-9] This makes validation of CFD results arduous, since most give pressure distributions. This prompted the addition of pressure ports along the aircraft, and they have been the only means of obtaining quantitative information about the flow field for the actual aircraft.[8] Pressure distributions have also been found using full scale wind tunnel tests, and subscale wind and water tunnel runs.

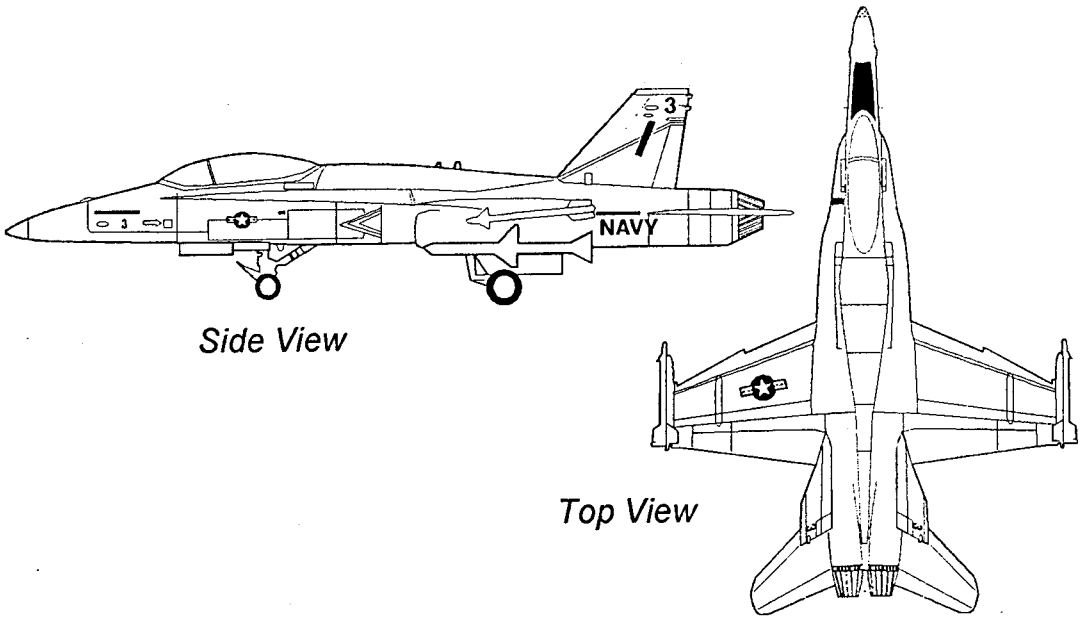

Fig. 1 F/A-18 Outline.

The correlation of pressure distributions on a full scale F/A-18 in the Langley 80-120 ft wind tunnel, however, do not always agree with the pressure distributions obtained in actual flight.[2] The results tend to be highly dependent upon the Reynolds number, and the angle of attack. At an α of 30° both the forebody and wing pressure distributions are in good agreement. As α is increased above 40° the suction peaks in the forebody and LEX area tend to differ substantially[2,8] Some of this disagreement is attributed to the lack of being able to simulate the flow through the engine intake ducts.

Similar results have been found between small scale wind and water tunnel results. The subscale tests give good understanding of the vortex structure and the dynamics of the vehicle at moderate angles of attack. Phenomena such as wing rock and reduction in lateral directional stability at high angle of attack have been detected.[10] As α is extended to 45° and beyond, pressure correlation becomes worse, and the asymmetrical behavior of the vortices vary.

The same story is found by comparing CFD results to those of the HARV flight tests. Good pressure agreement, along with details of the forebody and LEX surface flow patterns are possible up to 30° α, but the correlation begins to depart after that. Like the full scale wind tunnel test, CFD does not capture the suction peaks of the vortices.[3] The burst point locations for the vortices are another area for concern. Codes with high grid densities of around 1.7 million for the forebody and LEX section of the F/A-18 are able to determine the burst point at around $\alpha = 30°$, while a hybrid grid structure of only 0.9 million nodes is valid up to $\alpha = 19°$.[4] Of all of the methods, CFD currently provides the poorest prediction of flow at high α and this is most evident in the prediction of the tail buffet experienced on the F/A-18.[11] Prediction of such phenomena will require much higher grid densities along with longer simulated time records. [11] The most beneficial results, still come from the actual flight test aircraft. This fact is evident when comparing all three together (Fig. 2).

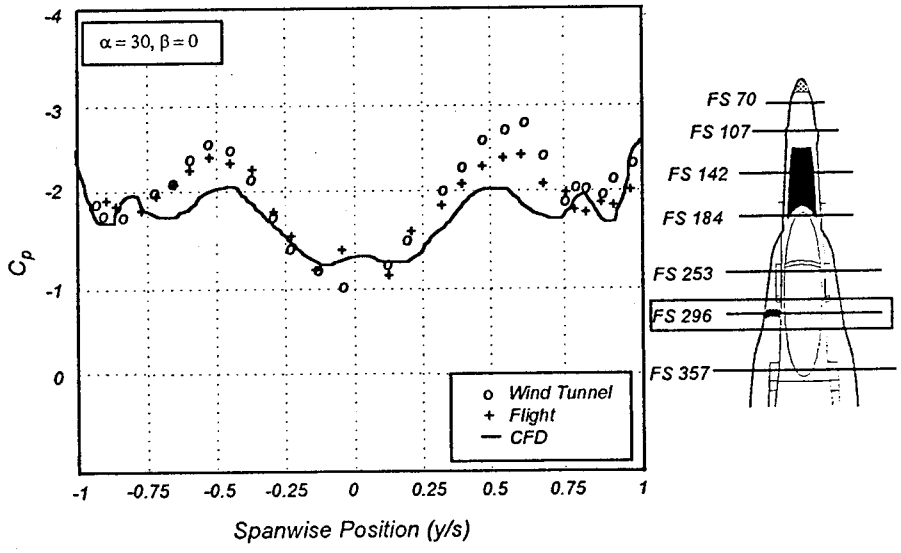

Fig. 2 Comparison of Flight, Wind, and CFD Results.[6]

For the most part, these tests have been conducted at steady state flight conditions, while fighter aircraft will be maneuvering in this flight region. Therefore the current thrust in the HATP is in the area of post stall maneuvering. Two methods are available, thrust vectoring and Forebody Vortex Control (FVC). The first method has already been demonstrated on the HARV, X-31, and the F-16 Multi Axis Trust Vectoring (MATV) aircraft which all use a form of thrust vectoring to produce a side force to compensate for a loss in stability and control effectiveness.[12,13] Not only does such a capability enhance maneuverability in a dog fight, but may allow for superior stealth design by completely or partially removing the vertical tail.[14] The vortices shed by the forebody and LEX are still important since asymmetrical vortices could produce stronger side forces than can be compensated by the thrust vectoring system. Therefore, the dynamic behavior of the vortices and the aircraft must be examined for these vehicles.

The last method of control uses these vortices to provide the necessary side force and moments to control the aircraft. To do so, one must be able to control the shedding of the vortices. The two most prevalent methods are blowing in the boundary layer or mechanical vanes.[15-18]

The utilization of blowing as a means of vortex control has already been demonstrated on the X-29. By using two high pressure air jets located on either side of the upper nose section, the controlled shedding of vortices at high AOA can be performed. By blowing air on the right side of the nose, the static pressure on that side is reduced which moves the right vortex closer to the surface. Entrainment of air blows the opposite vortex away, which in turn raises the pressure on that side of the nose. The net result is a side force to the right. This system provided added control power in roll and yaw for the aircraft up to angles of attack of 50°. The most

important result from the test was the existence of a time delay between when the jet is fired and when the actual moment is felt by the ship. This delay must be better understood to employ this type of system during high α maneuvering.[15]

The latter method of controlling vortex shedding is being investigated on the HARV by focusing on the application of actuated forebody strakes in the nose section.[18] Like pneumatic FVC, the program hopes to enhance yaw control at high angles of attack where conventional controls would become ineffective (Fig. 3).

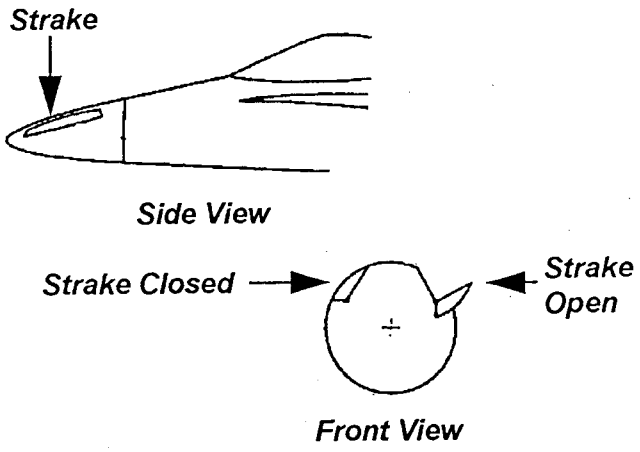

Fig. 3 HARV Nose Strake Configuration.[18]

Results from a 16% scale model utilizing the proposed system indicates that the FVC system will have as much control power at 40° α as the rudders do at 0°. The effectiveness of the system increases to an α of approximately 50° (Fig. 4). Testing has also verified that the system works well for a wide range of sideslip, Mach number, rotation rate, produces very little coupled rolling and pitching moments, and provides a well behaved variation of yawing moment with strake deflection.[18]

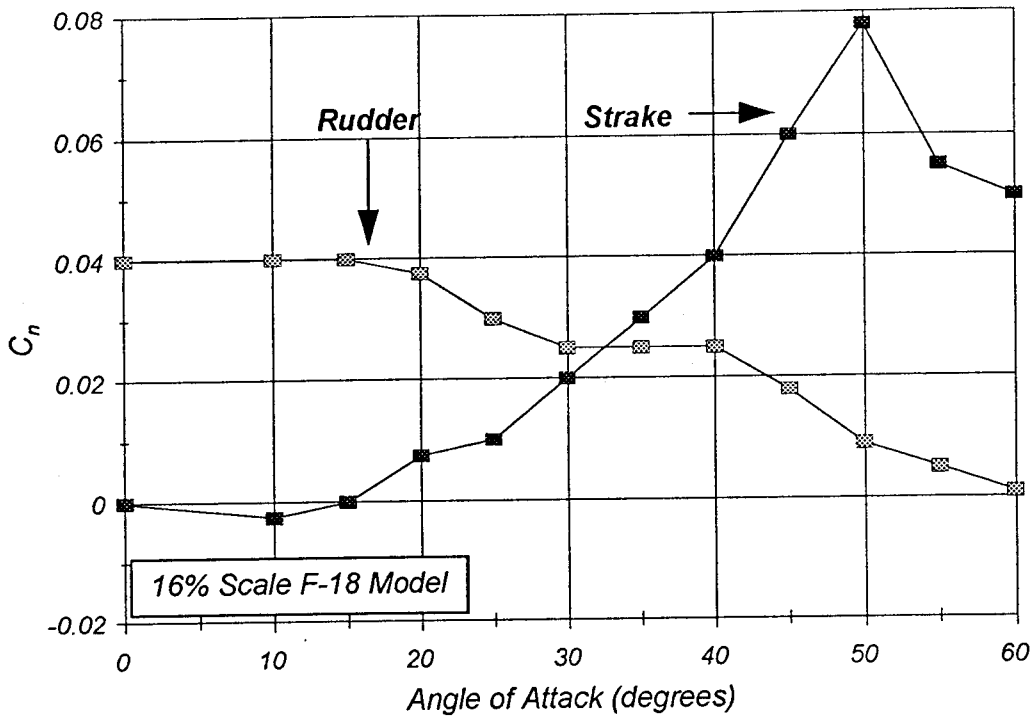

Fig. 4 F-18 Rudder and Forebody Strake Yaw Control Power.[18]

This type of FVC system requires that the characteristics of the vortices be understood in order to develop adequate control laws to take full advantage of the envelope expansion that FVC offers. As seen earlier, wind tunnel and CFD results become less reliable as angle of attack is increased. It is therefore necessary to derive as much quantitative data as possible from actual flight tests. Most flight test methods, unfortunately, do not lend themselves readily to providing good quantitative results of the position and velocity of the vortices during dynamic maneuvering of the fighter. Moreover, using pressure rakes and Laser Doppler Velocimetry on the aircraft on the ground does not tell the whole story, and these systems are too large and too expensive to carry in flight. Video imaging, however, may prove to be the

best solution. Currently Texas A&M's department of Aerospace Engineering is using a video tool called ExpertVision (EV) to determine the motion of a variety of targets.

The main advantage of using ExpertVision is that it is not restricted by the size of the test object, and as long as at least two cameras can "see" the event, a trajectory can be calculated. This calculation, however, rests on two underlying assumptions. First, one has to be able to see what one wants to track, and second, the cameras remain in a fixed position.[19]

The vortex is composed of air, which cannot be distinguished from the air around it. So, the vortex must be made visible with an in-flight smoke flow visualization system. The system currently on the HARV produces a visible, continuous vortex that can be seen by the cameras (Fig. 5), but there is no way to calculate the velocity of the vortex core. The smoke must be broken up into individual packets which can be tracked in order to obtain core velocity.

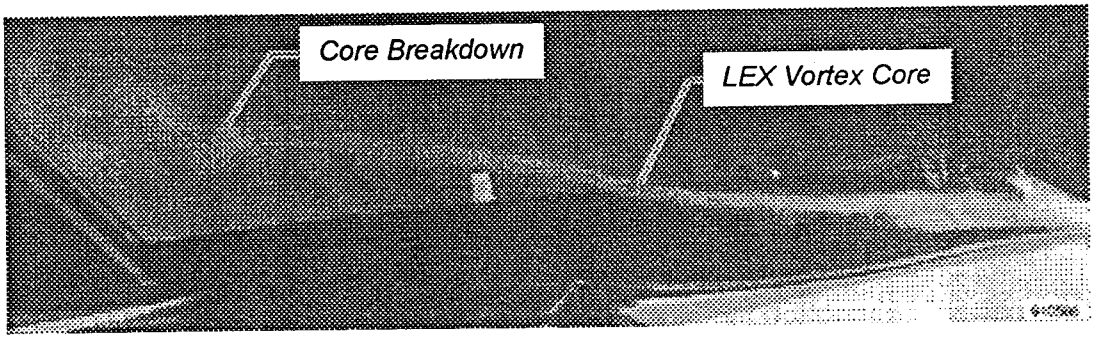

Fig. 5 Smoke Flow Visualization on the HARV.

Another problem associated with seeing the vortex is the angle of the cameras. Motion Analysis recommends that the cameras' lines of sight be orthogonal for the best accuracy. On the HARV, the only feasible locations are on the wing tip missile launcher, which provides a camera separation of only six feet. Such camera positions could produce unacceptable errors in the data.

The final area of concern is with camera motion. The EV system assumes that once the camera locations have been set that they do not move. Since the cameras for the flight test are mounted out on the wing tip, they will experience both translational and rotational motion due to wing bending and torsion during the dynamic maneuvers. This motion has to be compensated.

The first problem of tracking the vortex was solved with the use of an intermittent smoke flow system, which seeds the vortex core with distinct packets of smoke. A preliminary system designed by Myatt[20] and flight tested by Dorsett[21] on a Grumman GA-7 Cougar demonstrates that such an approach is feasible for the HARV.

The intermittent smoke flow device consists of a chamber to hold the smoke cartridge, a plenum chamber, and a shuttle valve. For the flight tests, a smoke cartridge is placed in the cartridge container and fired electronically. Smoke then flows into the plenum chamber, which helps to prevent severe pressure rises in the system that could be a flight safety hazard. The smoke then flows through a valve that alternately sends smoke to a waste outlet or to the leading edge vortex (Fig. 6). This method is used over simply blocking the flow to prevent any severe pressure rises in the plenum chamber, and to reduce the exit velocity of the smoke into the flow. The reduced exit velocity is important since blowing the seeding smoke into the flow at too high a velocity could change the characteristic motion and location of the vortex.

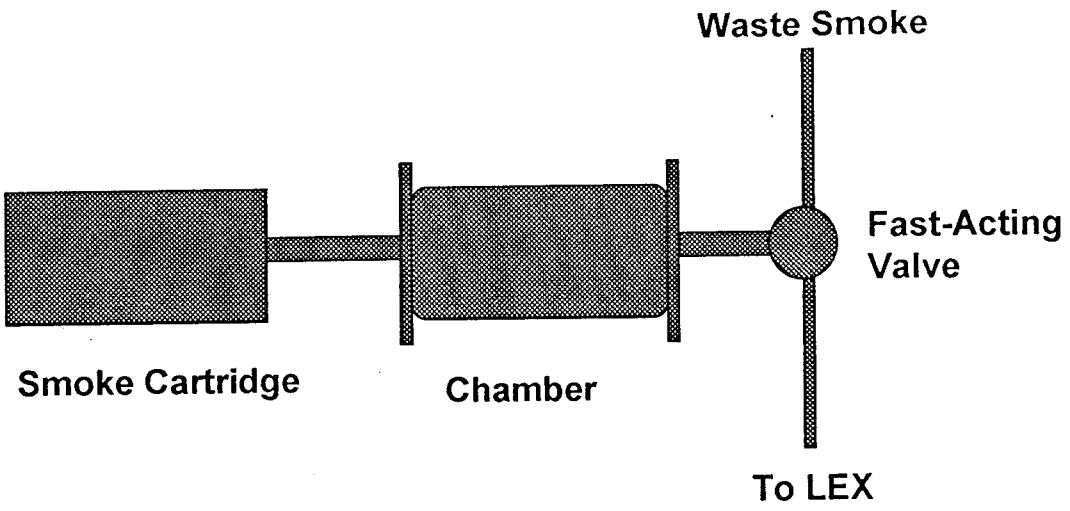

Fig. 6 Intermittent Smoke Flow Visualization System.

Ground testing by Myatt[20] proved that the system could operate reliably for multiple firings, and that distinct packets of smoke were produced. Testing of the system in the wind tunnel with a delta wing at a high angle of attack demonstrated that the system worked well for seeding a vortex core. Furthermore, the leading edge of the smoke packets remained intact until the burst location, which permitted trajectories to be determined by the system. These wind tunnel tests also showed that this method would not be suited for turbulent non-vortical flow, since the leading edge of each smoke packet diffused rapidly.

Flight tests demonstrated that the system produces visible smoke packets which can be tracked by EV in actual flight. The tests showed we were able to accurately determine the trajectory and axial core velocity of a vortex produced by a LEX at 22° AOA.[21] During this phase of the program, the cameras were placed in optimal locations to maximize the accuracy of the EV system. The data reveal that a high camera speed will be required to obtain enough data points to accurately determine the trajectory and velocity of the vortex on the HARV. NASA plans to utilize two high speed film cameras to capture the event.

The problems yet to be solved are those of camera motion due to the position of the cameras on the wing tip missile launcher rails, and a determination of the expected accuracy of the EV system. The correction of the smoke packets for camera motion will come from trajectories of fixed reference markers on the aircraft. An acceptable algorithm and data reduction technique must be developed, and its affect on accuracy estimated. The impact of the cameras position on system accuracy must also be assessed. These remaining problems are the focus of the following research.

EXPERIMENTAL EQUIPMENT AND TEST PROCEDURES

Overview of Experiments

To remove the motion of the cameras from the video data, a relative motion approach has been proposed. Fixed markers would be applied to the aircraft's fuselage and tracked along with the vortex smoke packets. After the flight, the trajectories of the stationary targets could be used to apply a correction to a vortex path, eliminating the effects of camera motion.

Before NASA will incorporate the intermittent smoke flow visualization system and ExpertVision in a flight test, the method must be proven on the ground, and the accuracy of the system must be estimated. This verification was accomplished with two ground based simulations with the video system. The first was a scaled down test, mainly to verify the feasibility of using relative motion to compensate for camera motion, and the second was a full scale mockup to determine the expected accuracy on the HARV.

For the first tests, a simple quarter inch plastic bead was tracked at a known velocity across a three and a half foot field of fixed targets. The test matrix consisted of runs to verify the ability to track while translating and rotating the cameras at the same frequency ratios of the F/A-18 wing bending and torsion modes.[23] During this phase, a systematic technique for smoothing and processing the data was refined along with an algorithm for correcting the motion of the cameras. The test was also utilized to verify the accuracy of two cameras in the same orientation as on the aircraft.

Finally, a full scale mockup was constructed. For the mockup, golf ball sized targets were placed along what would have been the LEX and fuselage of a F/A-18

Hornet, with the cameras located at the wing tip missile launcher. In this final phase, the accuracy of the EV system to locate known points on this scale was determined, along with its ability to track a known moving target on a circular trajectory towards the cameras and along the fuselage of the plane.

The ExpertVision System

The ExpertVision System is a 2-D or 3-D hardware and software video analysis package produced by the Motion Analysis Corporation. The hardware consists of two or more Fairchild-Weston high speed cameras, 200 frames/second (f/s), a VP320 video processor, a 13" black and white TV monitor, and a Sun color SparcStation 1+, produced by Sun Microsystems (Fig. 7). The Sun work station runs the EV software packages for data collection and editing.

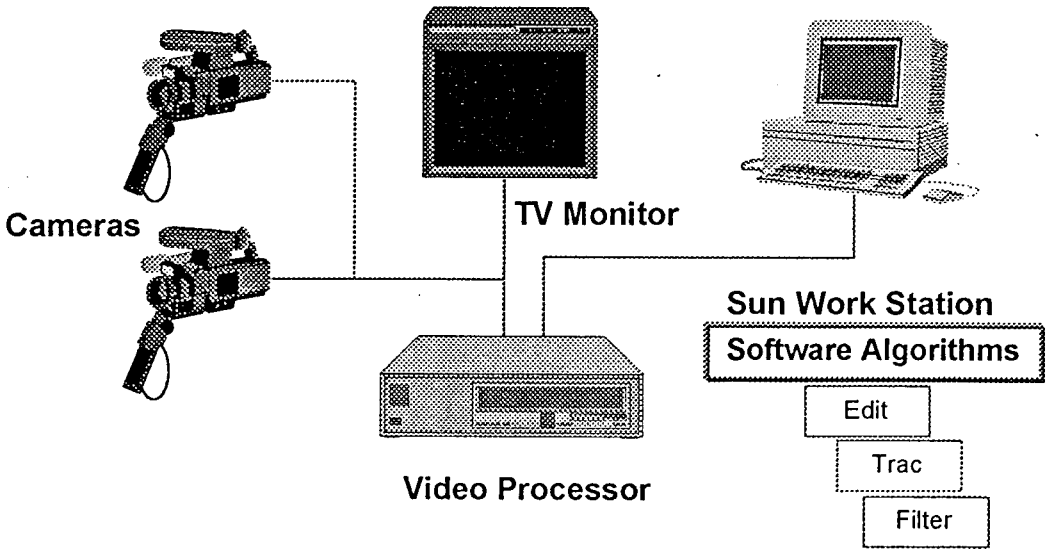

Fig. 7 Imaging System Components.

The VP320 video processor acts as the interface between the cameras and the EV software. The processor controls the synchronization of the cameras, and commands the sampling rate. The contrast between the background and the desired targets is selectable on the video processor and is viewed on the monitor. The processor also contains several features to improve the contrast levels between the background and the desired targets. These features consist of filters, masks, and editing windows. The processor then transforms the raw video data into a digital signal to be utilized by the software's programs.

Two software packages were provided with the system. The first called the Video Analog Collection (VAC), is used to collect data real-time. The VAC controls the duration of the data collection and provides a means of previewing the quality of each video file.

The software package EV3D performs data reduction from the video file produced by the VAC into actual trajectories. This program contains the necessary routines to calibrate camera position, perform frame editing of the video data, correct the camera lenses for errors, compute the trajectory of a target, and edit the subsequent position data.

Test Setup to Validate Relative Motion

Lab Test Board

For the first phase of the project, a simulated target was moved across a field of fixed markers. This task was accomplished with a black 4x1' plywood sheet with a slit cut down the middle length wise, and 12 quarter inch white plastic beads randomly attached across and above the board. These control points are numbered one through twelve on the board in Fig. 8. The simulated moving smoke packet was then made by attaching another bead by a wire rod through the slit to a trolley on rails that was fastened to the back side of the board (Fig. 8). This trolley was then connected via pulleys and a belt to a constant speed DC motor. A Tektronix CPS250 power supply was used to control motor speed.

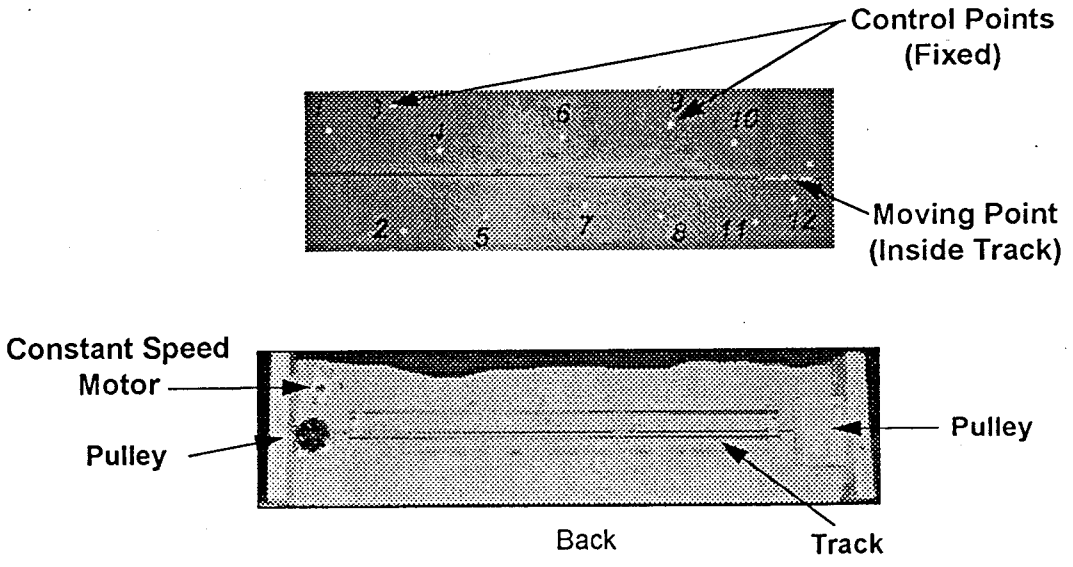

Fig. 8 Laboratory Test Board.

Attaching the trolley to the back side of the board reduced the chance for extra edges and targets to be seen by EV. The rails were made from 3/8" steel rods, to provide a rigid track for the Plexiglas trolley to move on. This rigid track eliminated any unnecessary motion from the trolley as the motor was turned on and off and limited the target to a known path.

The trolley was constructed from a 3" x 2 1/2" x 1/2" Plexiglas block. Two 3/8" holes were drilled down lengthwise for the steal rods to slide through. These holes were polished and then lubricated to reduce the amount of friction and provide for a smooth consistent travel (Fig. 9). There was some play between the trolley and rails, which was measured at approximately 0.01 of an inch.

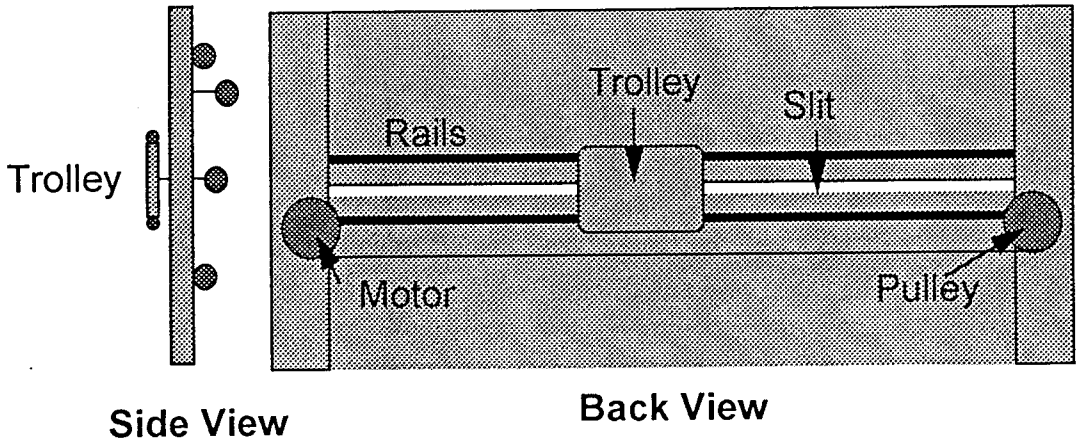

Fig. 9 View of Trolley.

The exact location of each of the fixed points and the trolley motion was determined by the use of a milling machine with an accuracy of 0.002 inches. The board was laid on the table and the left most control point taken to be the origin for

the rest of the board. A right handed coordinate system was used with the X axis running the length of the board, the Y axis up the width, and the Z axis out of the board plane (Fig. 10).

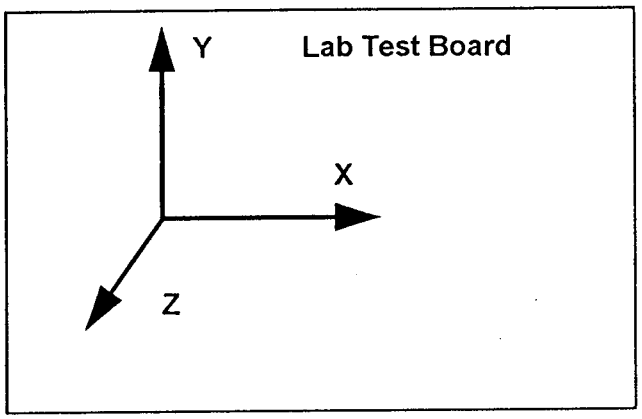

Fig. 10 Lab Test Axis System.

The Camera Shaker

The simulated wing tip motion of bending and torsion came from the modification of a platform used to perform flutter and divergence experiments in the wind tunnel at Texas A&M. The platform allowed a test object attached to it to translate and rotate freely, but springs were attached to limit the travel.

For this experiment a camera mounting system was constructed with a 28" x 3" aluminum C channel, and two wooden blocks. The channel was bolted to the platform, simulating the wing tip missile launcher. Two 1" x 3" wooden block were bolted to the end of the aluminum beam, providing a flat surface for attaching the two cameras. Between the wooden block and the cameras, strip of 1/16" rubber padding

was placed to prevent the cameras from slipping out of place while the system was in motion. Finally, the springs on the platform were adjusted to center and counterbalance the camera system (Fig. 11).

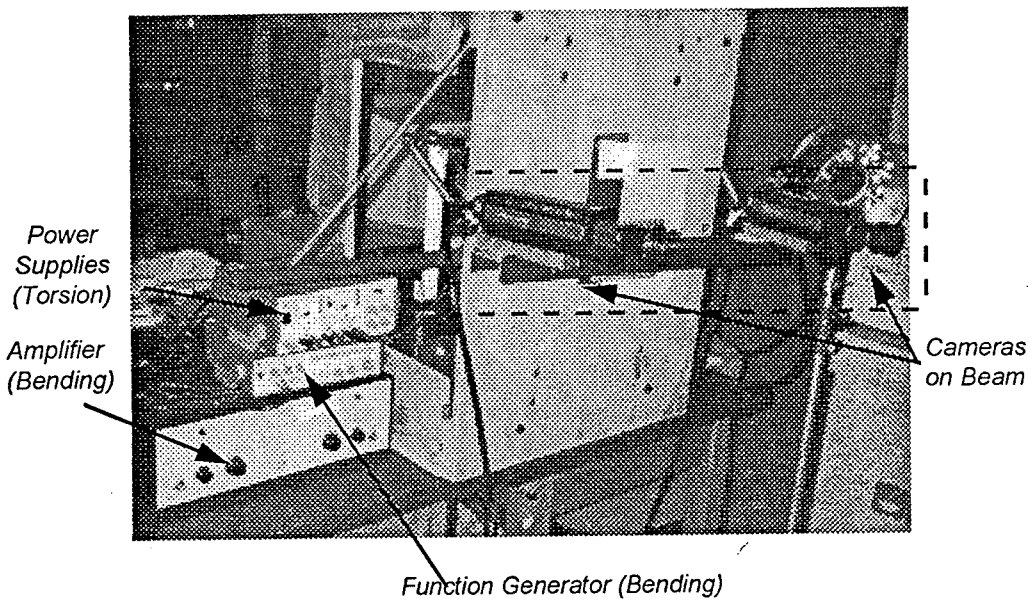

Fig. 11 Camera Shaker (Front View).

The platform also had to be modified to translate and rotate the camera assembly at a known frequency. This function was accomplished by attaching a B&K Instrumentation's Type 4809 Vibration Exciter to control the translation, and a geared electric motor and lever arm to handle wing torsion.

The shaker was bolted to the bottom of the apparatus and then to the carriage that moved to simulate wing bending. The bending motion was then controlled by the use of a Hewlett Packard 3311A Function Generator, which sent the desired signal to

a B&K Type 2712 Power Amplifier and then out to the shaker. This arrangement allowed the bending motion to be controlled separately from torsion.

The motors responsible for wing torsion were bolted to the translating carriage assembly. A constant speed geared motor was utilized to power a lever arm which moved up and down. This lever arm was then attached by an aluminum bar to a large Plexiglas flywheel. This wheel was attached to the camera beam via a metal drive shaft. As the lever arm moved up and down, the flywheel rocked back and forth, which caused the camera beam to oscillate, simulating wing torsion (Fig. 12). The frequency of this operation was controlled with a Hewlett Packard DC power supply, and measured with a strobe light. The magnitude was set to allow for the cameras to maintain all of the targets in their fields of view.

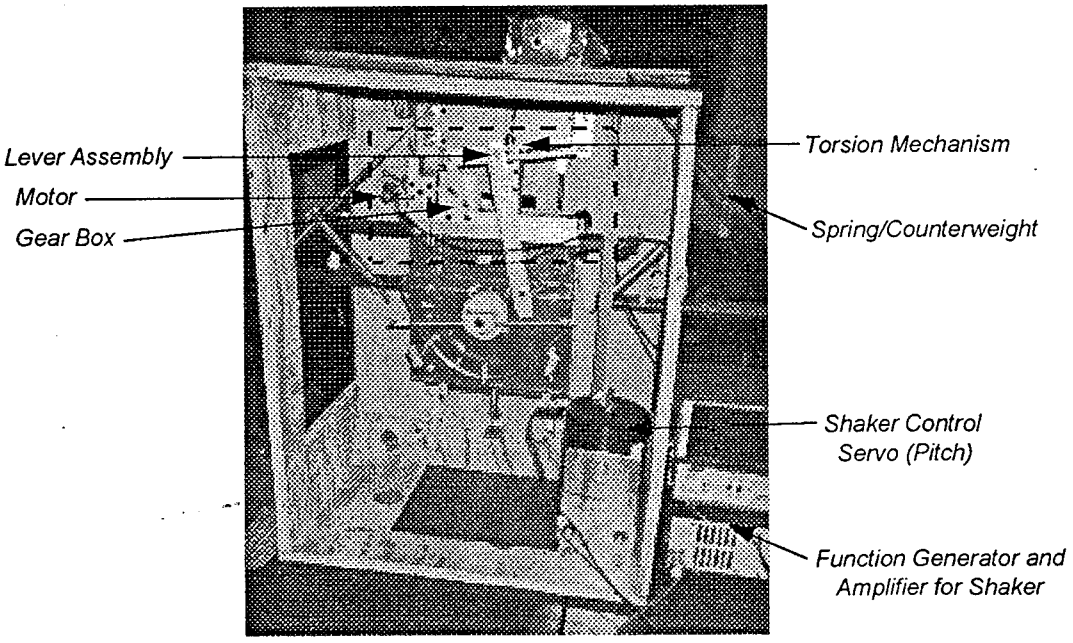

Fig. 12 Camera Shaker (Back View).

Test Procedure

The camera shaker apparatus faced the test board in a similar orientation as planned for the HARV. The distance between the cameras and board was set by filling the cameras fields of view. This arrangement allows data to be collected about accuracy across the system's field of view, and yet closely simulates the conditions for the actual flight tests.

The test matrix consisted of tracking the moving target at various speeds with the cameras stationary, simulating wing bending only, wing torsion only, and then a combination of the two. The frequencies for wing bending and torsion were set at 1.2 Hz and 1.5 Hz respectively, thus retaining the same frequency ratio between the two modes of motion as found on the HARV.[22] It was necessary to use a lower frequency in the lab due to the slower camera speed, and the physical limits on the shaker camera combination. The final test using this board worked with changing orientation of the board to assess the effects of resolution and / or focus on accuracy.

For all the tests conducted, data were collected indoors at 200 frames/second, which dictated the use of artificial lighting to provide sufficient contrast. Before each run, two seconds of stationary data were collected to calibrate the camera location points. Then the cameras were set in motion for the desired test, the cameras were turned on, and finally the moving target was sent across the board. After each run, the video data files were inspected with the VAC viewer to make sure the run was captured.

Once the data files were digitized, the EV3D software was employed for the first stage of data reduction. Before a target can be tracked, EV must know the location of the cameras. Their position is found using the calibration data collected before each run, and the CALI subroutine in the software.[19] The location of at least six non-coplanar points is input to the system, and then identified in each camera's field of view through a graphical user interface. The output from the CALI routine is an environment file, and the norm residuals. If the norm residuals for a calibration are lower than 1, the calibration is considered to be valid. For all calibrations this value was less than 0.35. Once the cameras were calibrated, this procedure did not have to be repeated unless the camera system was moved.

With a valid calibration, the TRAC subroutine is then employed.[19] In this routine targets are selected that need to be tracked in one of the camera's field of view. The software then located the corresponding target in the other two camera windows. A beginning frame was selected along with a stopping point, and the software returned coordinates for each target over time.

The TRAC routine, however, failed to maintain a lock on each target for the data runs where the cameras were moving. As the cameras moved EV could not find the correct corresponding points in the other camera's field of view, and would mix and match targets together. To get around this problem, the video editor MASK was utilized to erase all but one target for the data run in each window. TRAC was then used to obtain its trajectory, and then the whole process was repeated for the remaining points.

After the trajectories for each target were obtained, they were examined with the TRED subroutine.[19] Here gaps in the data could be seen, where EV had lost the target for one or two frames and then picked it up again. The JOIN command connects the trajectory to fill any gaps that occur. Most gaps were only one to three frames, with the largest being seven. The trajectories were then written to ASCII files to be used by a personal computer for smoothing and to apply the relative motion algorithm. The TRED routine contains a filter option, but the Motion Analysis Corporation does not provide a great deal of information on what type of filtering is occurring. This, along with the need to perform a relative motion correction, prompted the use of MATLAB, a numeric computation software package, to be employed.[23] The software package contains a signal processing toolbox, which allows custom filters to be constructed and applied.

The data were filtered in MATLAB by first picking a cutoff frequency for the data by analyzing the spectral density plot. The cutoff point was selected to remove unwanted noise, while retaining information on the event. For all the runs an 8 Hz cutoff frequency was used to create a forth order digital Butterworth filter. Higher order filters did not seem to affect the data, and only added to the computational time. The Butterworth filter was selected for its ability to smooth data, but did sacrifice rolloff steepness for monotonicity in the pass and stop bands.[19] The data were then filtered both forward and backward to prevent introducing any type of phase shift to the data.

Relative Motion Algorithm

For test runs where the cameras were moving, a relative motion algorithm was applied to correct the trajectories of the interested targets. This subroutine had to be capable of correcting the data for both rotational and translational motion.

The routine utilizes the relative motion of two fixed points to apply a rotation and then a translation to the moving target. The routine is given the location of two fixed points, the time history of both of these points and of the moving target. At every frame, the routine calculates the relative angle between the two fixed points, and subtracts from it the known angle between the two points. The difference in the two angles represents the amount of rotation that has occurred due to camera motion at that instant (Fig. 13). Next, the angle and distance between the first point and the target are calculated. The opposite rotation is then applied by subtracting the camera rotation angle from the angle between the fixed point and the target (Fig. 13). By multiplying the distance between the control point and the target by the cosine and sine of this angle, a new X and Y coordinate are found for the target. This location, however, is based from the control point. To correct this, the actual location of the control point is added to the new coordinates. Not only does this return the target to the coordinate system of the board, but also corrects the target for any translation caused by the movement of the cameras (Fig. 13).

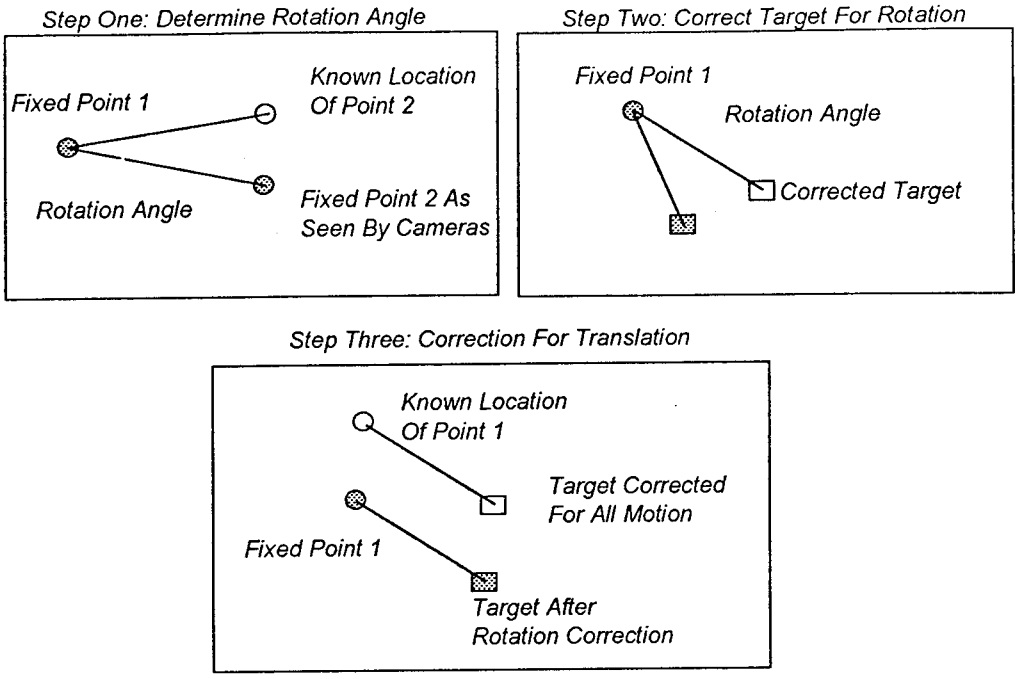

Fig. 13 Relative Motion Algorithm.

The relative motion algorithm was written using the MATLAB programming language. This allowed for both the filtering and correction to be done at the same time. The PLOT command from MATLAB allowed for a graphical representation to be obtained at the same time. A listing of this code is located in Appendix A.

Full Scale Mockup

The full scale mockup used to determine the accuracy of the system on the HARV was setup inside Texas A&M's Flight Mechanics Laboratory hanger. The model consisted of 13 practice golf balls placed at different elevations from 0 to 5' over a 23' x 5' section of floor. The locations for the balls were selected to simulate feasible locations on the HARV vehicle (Fig. 14). The area covered was equivalent to

the area just in front of the LEX and all the way back to the vertical tails. Each ball was suspended in air by placing it on a black wooden dowel of the appropriate length. The other end of the dowel was glued into a wooden base. The area behind and below the test setup was covered in a black felt material to improve the contrast between the balls and the surroundings.

To simulate a smoke packet an additional ball was mounted on a horizontal 2' rod that was driven by a constant speed motor. This rig produced a circular trajectory towards the cameras located on the wing tip (Fig. 14). The velocity of the target was again controlled through the use of a variable power supply. The velocities tested ranged from 4 feet per second up to 16 feet per second, which was the maximum obtainable with the motor.

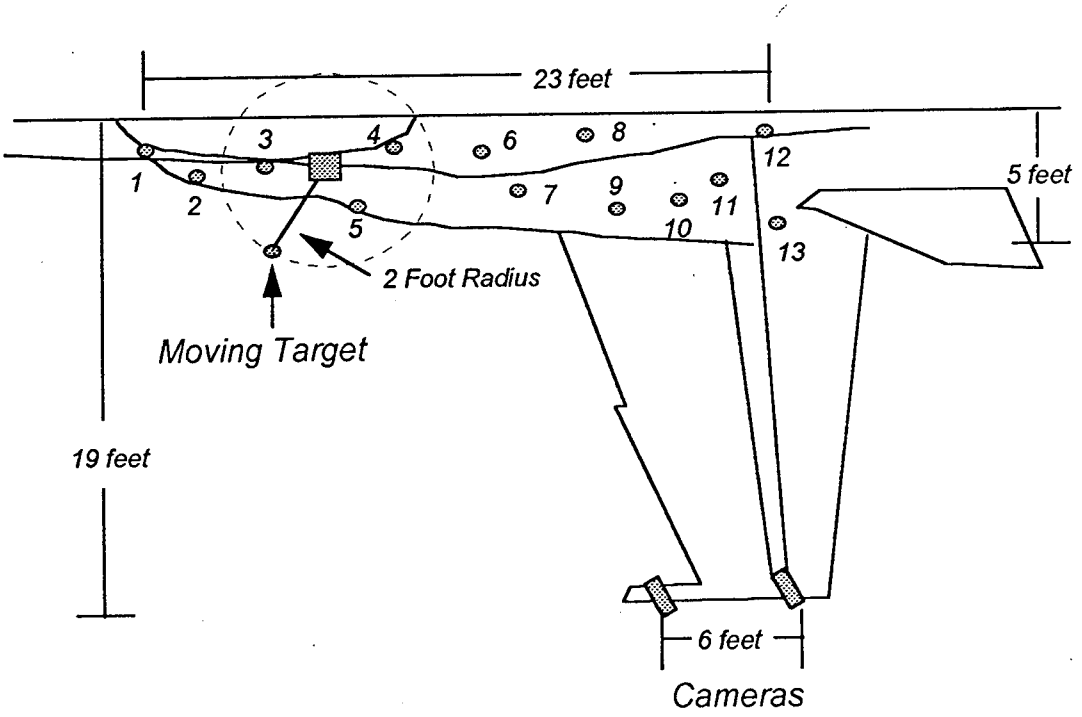

Fig. 14 Location and Numbering of Targets on Full Scale Model.

The major challenge in setting up this portion came from locating the fixed points and the moving smoke packet with respects to a coordinate system. Another right handed system was chosen with the positive X axis being parallel to the fuselage from the nose to the tail, the Y axis out towards the wing, and the Z axis down toward the landing gear (Fig. 15). To locate the points, a surveying transit with an 15 second accuracy was employed. The transit was placed at six locations along the floor, and the angle to each point measured, along with the distance and angle between the transit locations. With this information, the law of sines was employed to calculate the distance from the transit location to the point (Fig. 16).

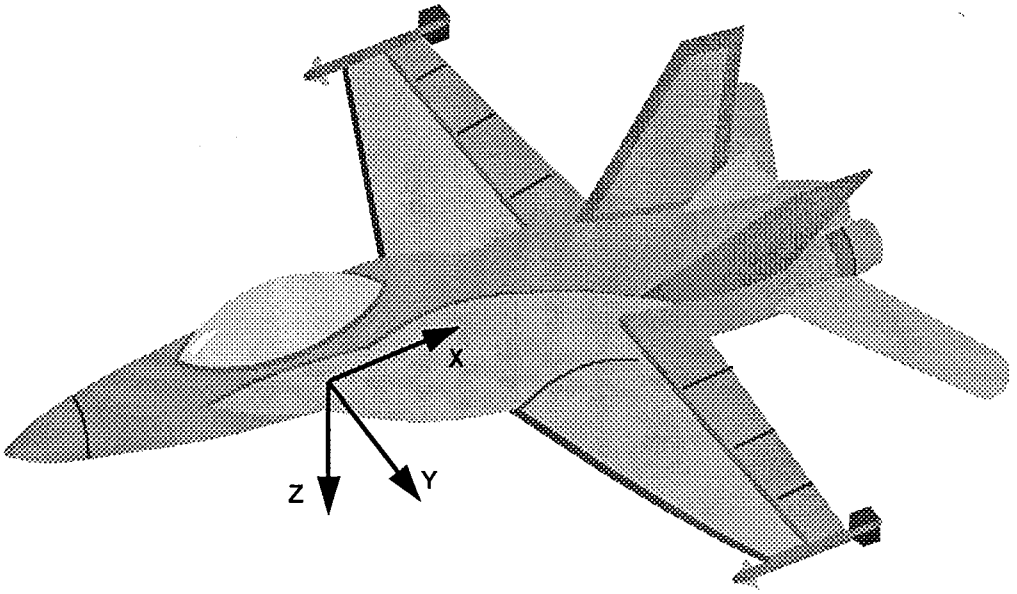

Fig. 15 Full Scale Mockup Axis System.

The X And Y coordinates for that point were calculated by multiplying this distance by the cosine and sine of the angle between the transit locations and the point. The Z location came from multiplying the distance to the point by the tan of the elevation angle (Fig. 16). The coordinates derived from each pair of transit locations were then averaged together to reduce possible errors in the measurement of the angles.[24] The final uncertainty in the location of the points using the above setup was 1.1 inches.

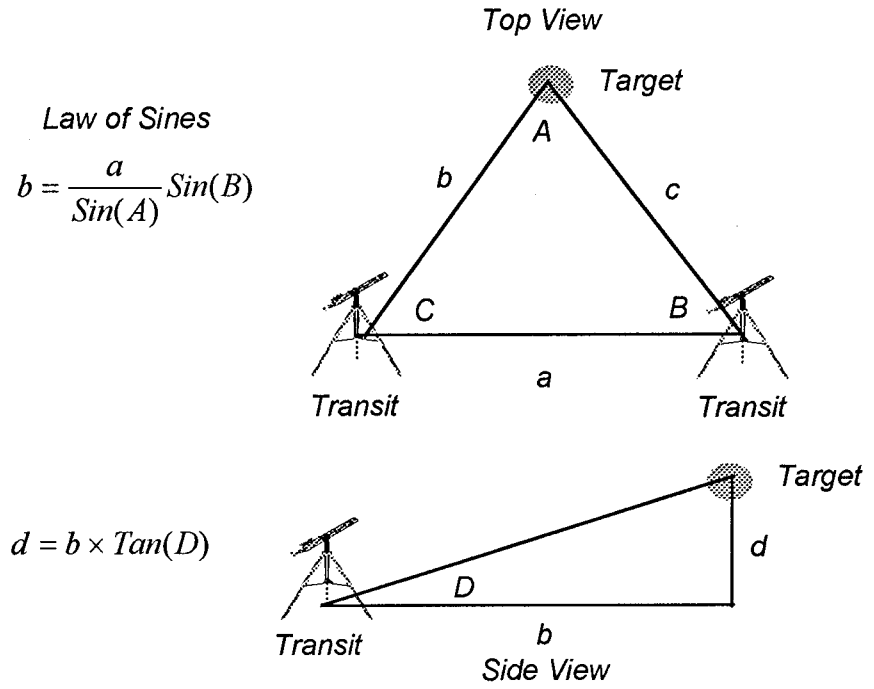

Fig. 16 Locating Target Coordinates with Transit.

The test matrix for this portion of the test dealt with varying the targets speed from 4 ft/sec to 16 ft/sec, and the focus location in the field of view. The cameras

inertia caused by a longer camera separation. The data reduction portion for this phase of the test was identical to the one applied in the small scale lab tests.

RESULTS

Stationary Camera Results

The first data runs presented here are representative samples of the data collected with the cameras stationary. The complete data files are provided on a floppy disk in Appendix B. The primary objective of these data was to quantify the accuracy of the system with two cameras that were almost parallel to each other and moving. All tests in this section were conducted at the Texas A&M Flight Simulator room with the small test board and cameras mounted on the shaker.

The first graph compares the trajectory of the moving target across the board with that of the expected trajectory (Fig. 17). As stated earlier, the data were filtered with a 4th-order Butterworth filter with a cutoff frequency of 8 Hz. The slight wavy appearance is due to errors in the EV system and actual play in the mechanical trolley itself. The largest difference between the nominal track, and that calculated by EV was on the order of 0.02 inches. One should also note that the track is in best agreement from 11 to 21 inches. This area represents the best region of focus for the cameras over their field of view. The camera position places the lenses much closer to one end of the board than the other. This makes it impossible to focus all of the control points.

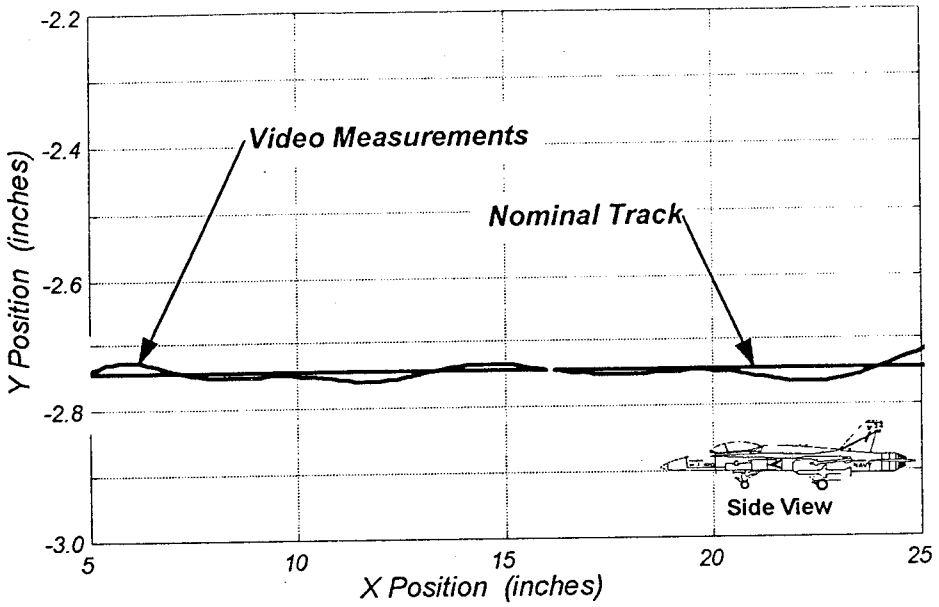

Fig. 17 Stationary Cameras - Trajectory of Moving Target.

Fig. 18 examines the accuracy of the system's depth perception with its reduced stereo vision capability due to the placement of the cameras. The EV system uses the difference in angles between the two cameras to determine depth and not changes in size. Cameras close together limit the accuracy of the system in this area. There is a large reduction in the ability of the system to accurately track the simulated smoke puff (Fig. 18). The maximum uncertainty in the measurement is more than an order of magnitude greater than that found in the XY plane. The mean error for this measurement is 0.133 inches compared with 0.002 inches for the XY plane. One should also note that the system's accuracy improves as the target moves into the focused region. The system's precision is also affected. The increased amplitude of

the oscillatory motion indicates a decrease in precision. The standard deviation grew from 0.011 inches to 0.127 inches.

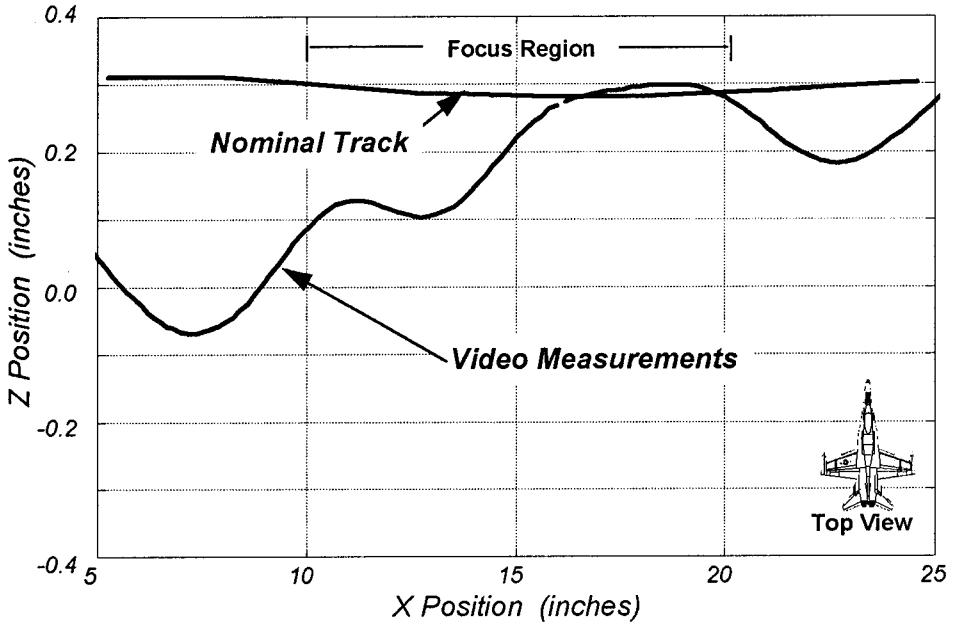

Fig. 16 Stationary Cameras - Trajectory out of Plane.

The next step was to evaluate system performance in determining the velocity of the moving target. The nominal velocity points are obtained by counting the number of video frames it takes the object to move between fixed markers. Since the distance between each marker is known, as well as the time interval between each frame (0.005 seconds/video frame), an average velocity for that distance can be found. This average was compared with the velocity calculated from the EV time history of the target. The velocity for the target is found by using a five point Lagrangian numerical differentiator on the data. The velocities for the beginning and

end of the data are determined with the use of a forward and rearward difference, respectively.

EV gave an excellent prediction of the velocity of the target as it accelerated from rest at the left side of the board and moved to the right (Fig. 19). The ability of EV to provide continuous predictions on velocities of a dynamic system is a valuable asset in analyzing a vortex.

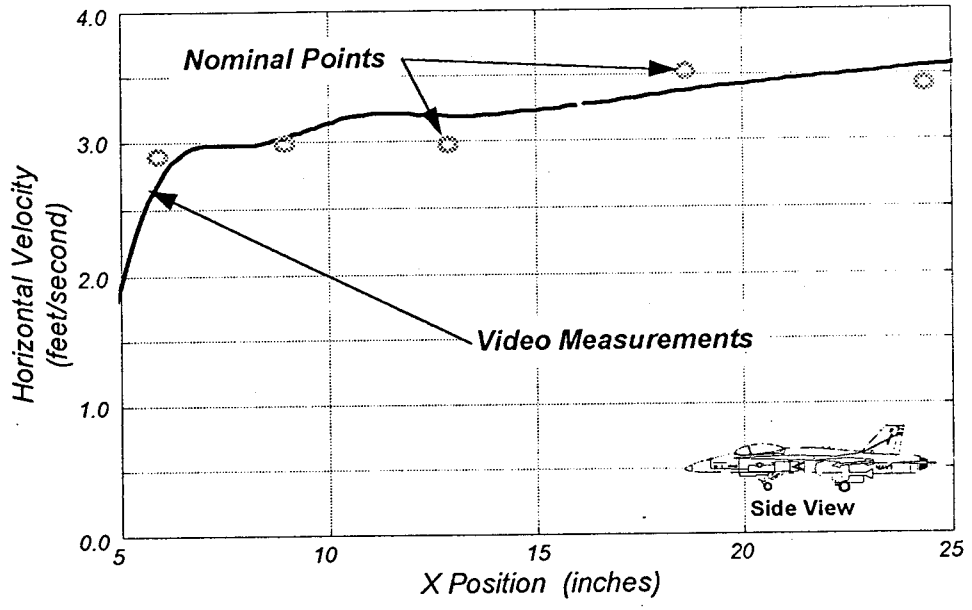

Fig. 19 Stationary Cameras - Horizontal Velocity.

The same numerical differentiator is again used estimate acceleration. The approximate acceleration history comes from the nominal velocity time history. This numerical method did not capture the dynamics of the particle starting from rest and moving across the board. The whole event took under one second to occur. EV, however, did capture some of the essential information about the acceleration of the

trolley from rest (Fig. 20). The EV track actually shows the high initial acceleration experienced by the trolley starting from rest. This again demonstrates the advantage of EV during dynamic flight test.

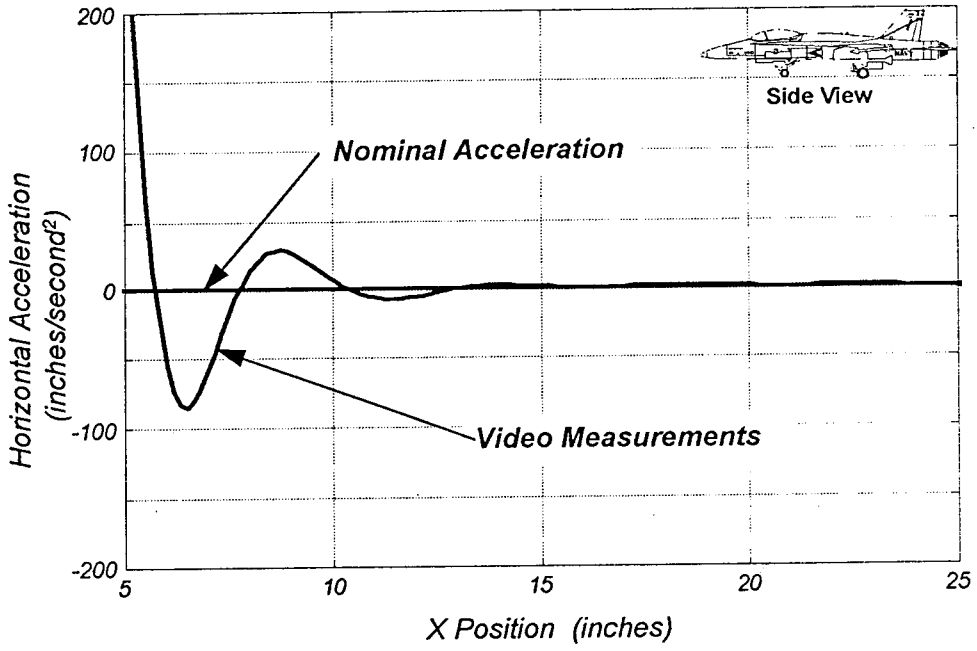

Fig. 20 Stationary Cameras - Horizontal Acceleration.

The vertical velocity of the trolley is zero since the track follows the X axis. This expected result is also confirmed by the data collected (Fig. 21). The average error in vertical velocity is 0.02 ft/sec with a standard deviation of 0.04 ft/sec.

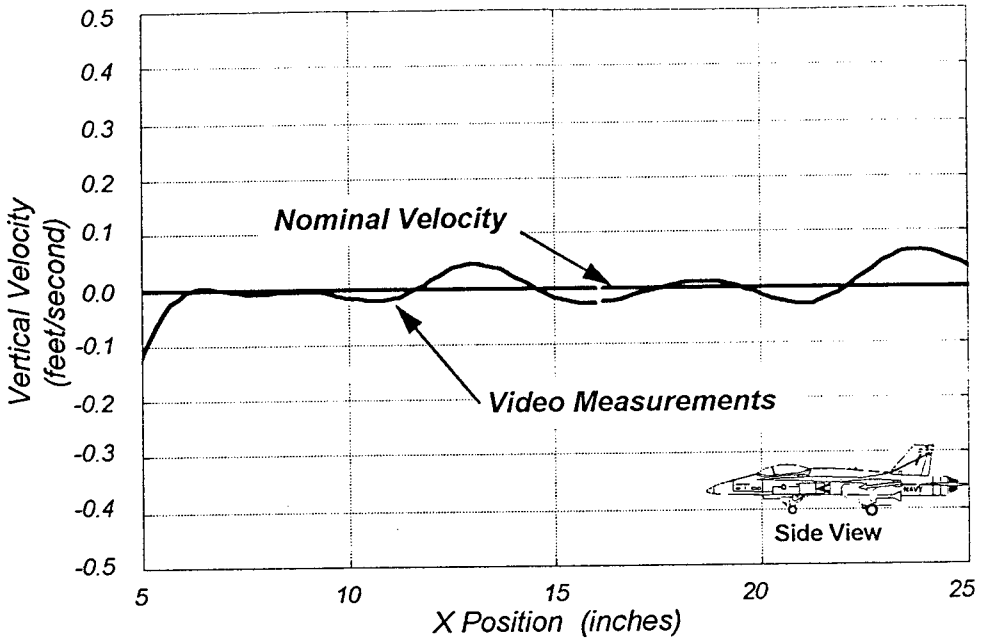

Fig. 21 Stationary Cameras - Vertical Velocity.

The next graph illustrates the decrease in accuracy for motion toward the cameras (Fig. 22). The bead moves in the XY plane, so the velocity in the Z axis should be zero. One can see that at one point in the run, the video measurements provided a velocity of almost 0.5 feet per second. These results continue to demonstrate the importance of camera location for the test. With nearly parallel lines of sight, the stereo effect of the cameras diminishes.

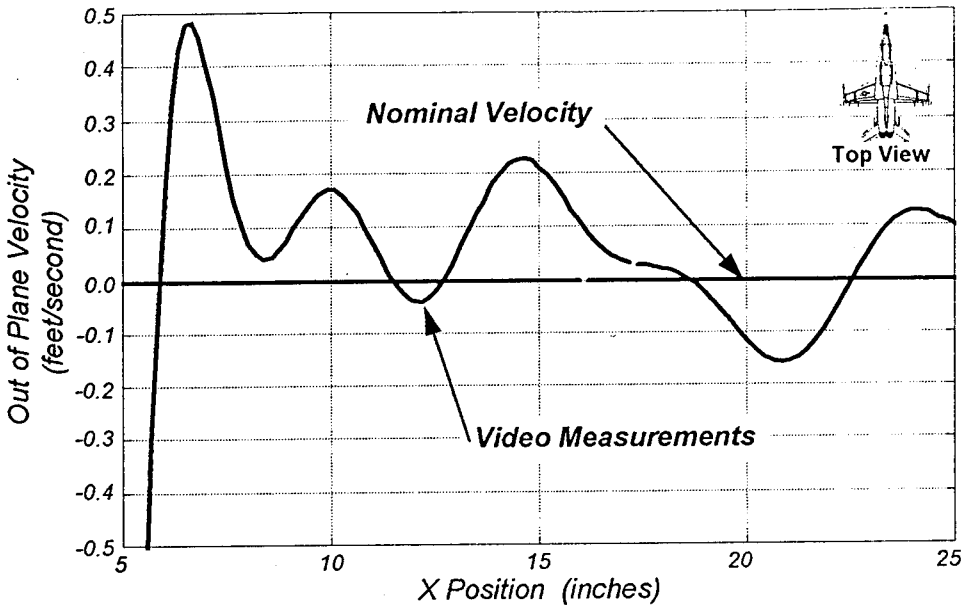

Fig. 22 Stationary Cameras - Out of Plane Velocity.

As stated earlier, it was impossible to focus the entire field of view due to the orientation of the cameras, therefore only the center area of the board was in good focus. The rest of the points were slightly blurred. From these results, it appeared that this reduced accuracy of the system in these regions. The focus area is depicted on the next page as a reference between control point numbering and the focus area (Fig. 23).

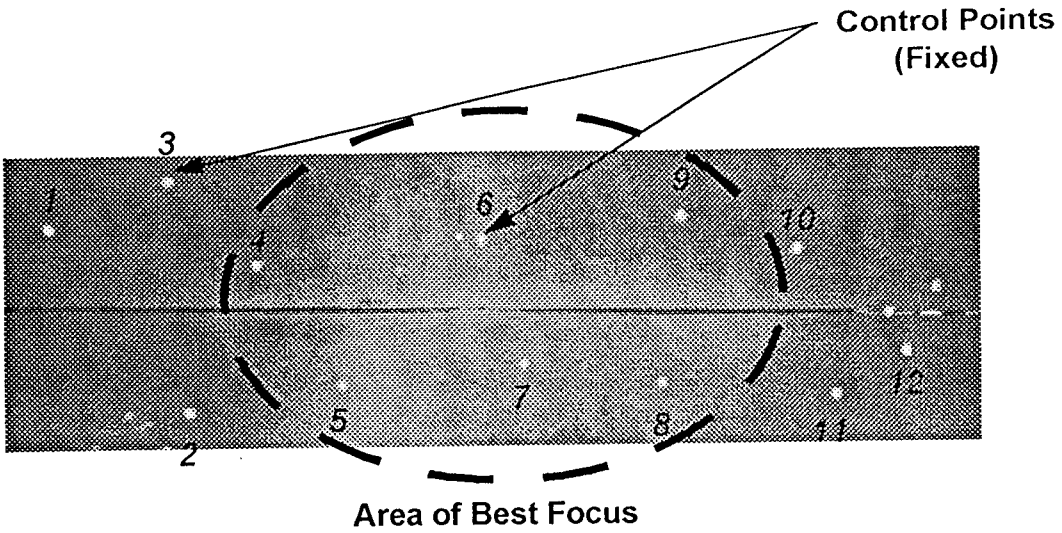

Fig. 23 Focus Region on Test Board.

The next graph compares the relative errors for the control points across the board (Fig. 24). Control point six is in the center of the region of the best focus for the test, and contains the least amount of error. Moving away from this area increases the error with the distance from point 6. Point 10 lies at the boundary, and has a slightly larger relative error than six. Point one, which lies the farthest away from the area contains the greatest amount of error. The greatest uncertainty for the points out of focus appears to be mainly in the horizontal direction.

It should also be noted that according to the data, the locations of each of the control points is not constant. This movement provides an indication of the precision of the system. The run represented 0.7 seconds of data, and the movement was caused by uncertainty in the EV system, as well as a phenomena called pixel twinkle.

Very small variations in lighting change the contrast of the target and the background. This fluctuation causes the edge of the object to appear to be moving

or to change shape. Either will cause a slightly different centroid to be calculated by the system. The system bases the location of the object off of its centroid. As the centroid moves, so does the location of the target.

The movement, however, is mainly in the horizontal direction of the board as appose to the vertical. This bias may result from different pixel densities for the two axes, the lighting in the room, camera position, and the focus region.

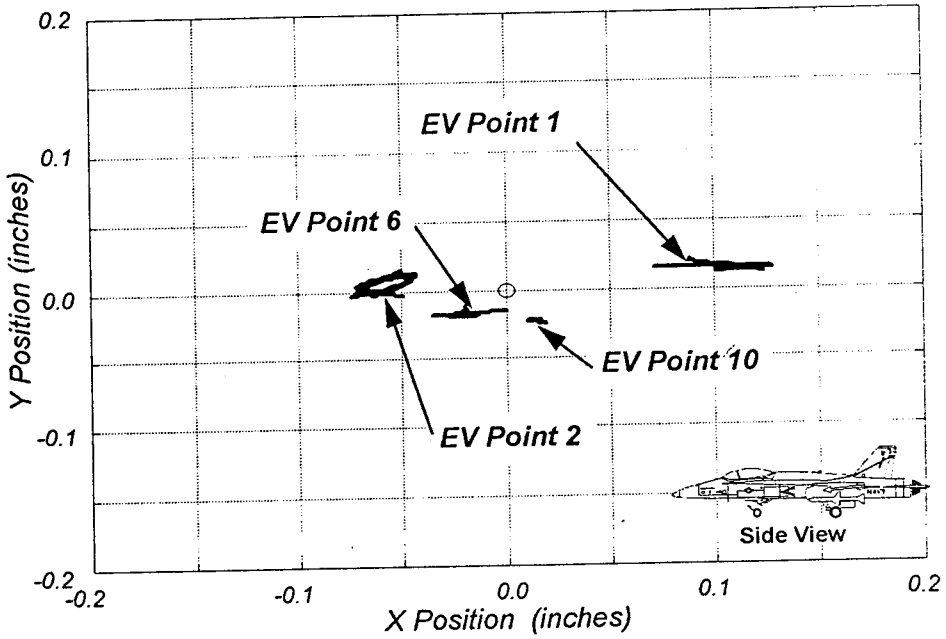

Fig. 24 Stationary Cameras - Relative Errors.

The next two charts compare relative errors between each axis for a control point in the focused region, and one outside of the region. Point 6 represents the control point in focus (Fig. 25). Again, the uncertainty of the Z axis measurement for the control point is an order of magnitude greater than for either X or Y axis. The

large fluctuations in the Z axis indicates a reduction in precision for this measurement also.

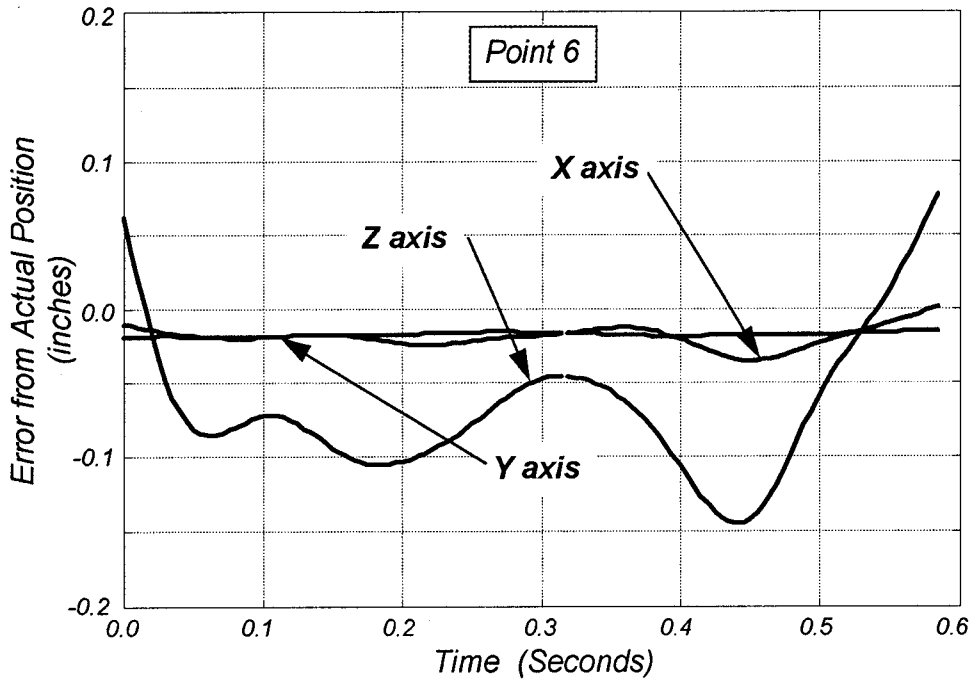

Fig. 23 Stationary Cameras - Errors at Point 6.

Point 11, on the other hand, is located out of the focus region. The uncertainty in the XY plane increased five fold from that of the point in focus to around 0.05 inches, while the out of plane error doubled from 0.1 inches to 0.2 inches (Fig. 26). Point 11 again illustrates the decrease in precision for the out of plane measurement with the increase in the variation of the Z axis. The standard deviation for out of plane measurements is 0.14 inches compared with 0.07 inches for those in plane.

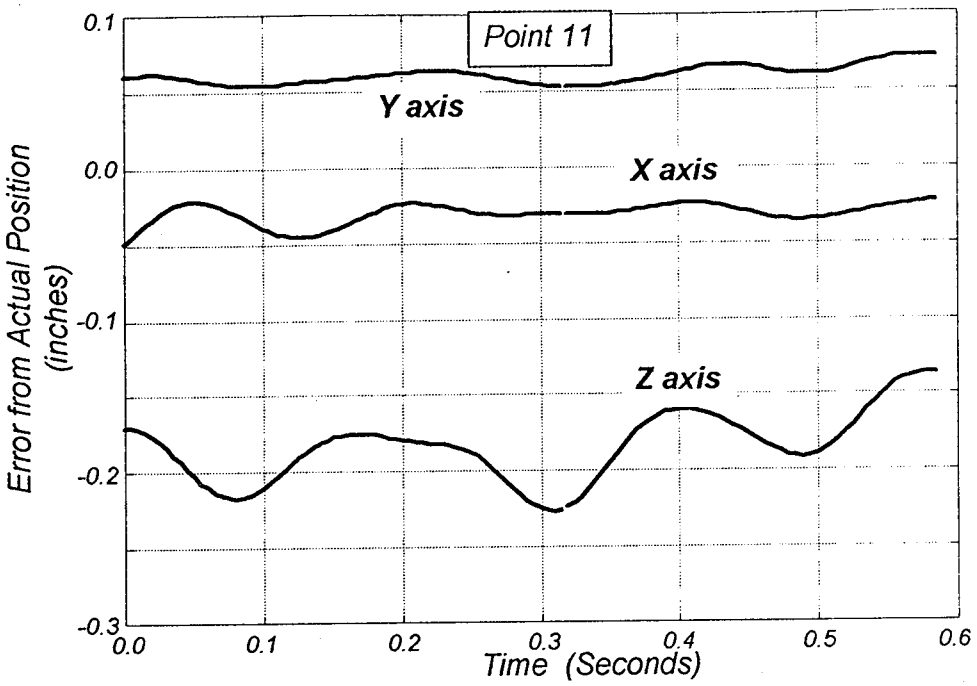

Fig. 26 Stationary Cameras - Errors at Point 11.

For the most part, the greatest uncertainty in the XY plane is along the X axis. To examine some possible reasons for this error, the board was rotated 90 degrees and data taken. The axis system remained the same with respect to the cameras, therefore, the Y axis was along the length of the board, and X paralleled the width of the board. The results show that the error rotated with the board (Fig. 27). This procedure discounted the notion that lighting or the camera position was the primary cause for the observed errors. How well points were in focus apparently dominates the error. Point 10 and 6 were in the focus region, and contain the least amount of error. Points 1 and 2, however, were out of focus and contain the most error. Point 1 was the only out of focus point that had more error in the X axis than the Y. This

indicates that other factors play into the accuracy of the system, like camera calibration.

The precision error however does not rotate 90 degrees as did the uncertainty. The points trace all remained flat with only a slight rotation noticeable (Fig. 27). This result underscores the fact that precision is mainly influenced by the lighting and camera position.

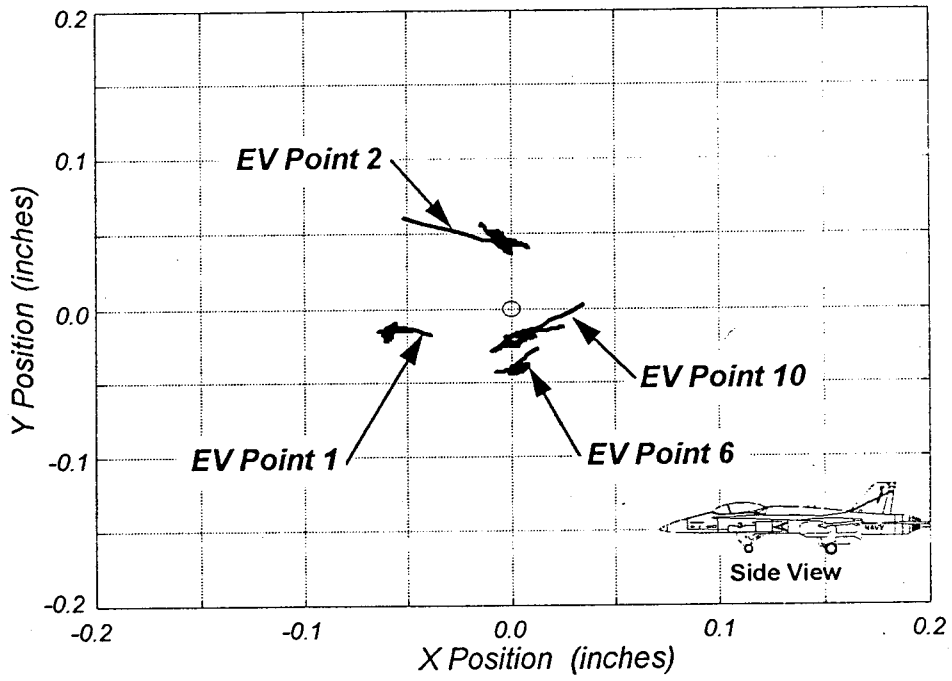

Fig. 27 Rotated Board - Relative Errors.

Moving Camera Results

The test setup remained the same as for the stationary camera run except that the cameras were translated and rotated to simulate the type of motion expected on

the HARV. A build up approach was taken with the cameras first translated, then rotated, and finally both motions combined. The same frequency ratio as the first bending and torsional modes on the HARV were used. This came out to be 1.2 Hz and 1.5 Hz between the first bending and first torsional modes.[23] All of the results presented in this thesis are for the combined motion. The data files for the other runs with each motion isolated can be found in Appendix B. The data reduction is the same as before except that the relative motion algorithm corrects the trajectory data before velocity and acceleration are calculated. This is accomplished by providing the algorithm the exact location of the two fixed reference point, their time histories, and the time history of the target to be corrected.

Fig. 28 depicts the trajectory of the particle in the XY plane before and after it was corrected for the motion of the cameras. The motion of the cameras significantly distorts the position information. However, the relative motion algorithm succeeds in removing this distortion. The maximum uncertainty of 0.045 inches for the corrected path was slightly more than double the 0.02 inches found in the stationary camera results.

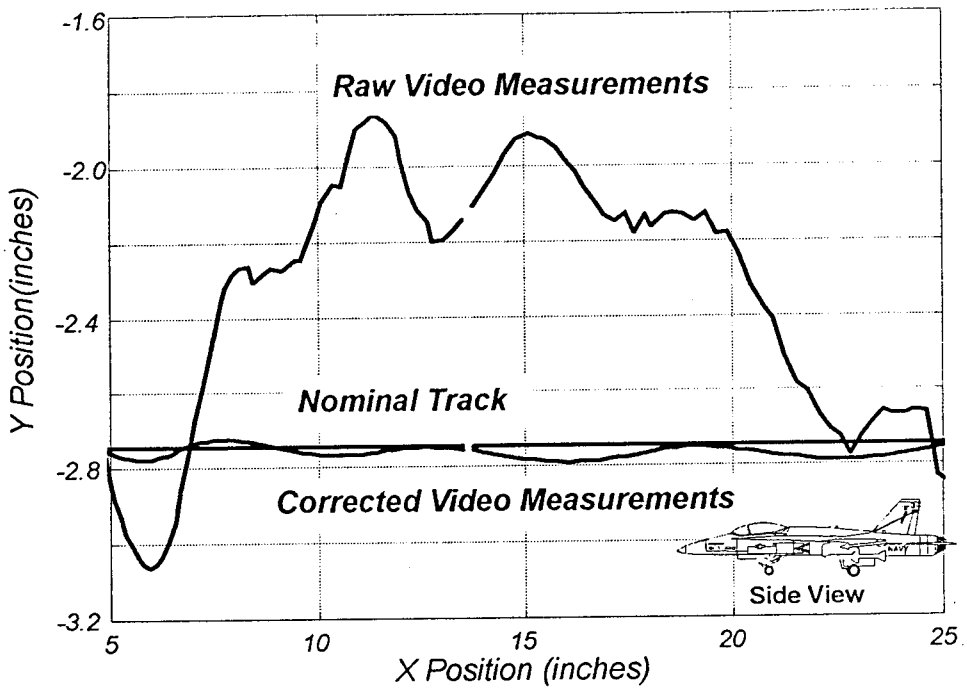

Fig. 28 Moving Cameras - Target Trajectory.

Just as with the stationary cameras on page 31, the accuracy of the system is significantly reduced in determining the location of a target on the Z Axis. The application of the relative motion algorithm did have an effect on correcting the data (Fig. 29). The corrected path is closer to the nominal track, by an average of 0.143 inches. Also as before, the trajectory becomes closer to the actual track as the target moves down the length of the board. The algorithm does not have a significant impact on improving the precision for the out of plane motion.

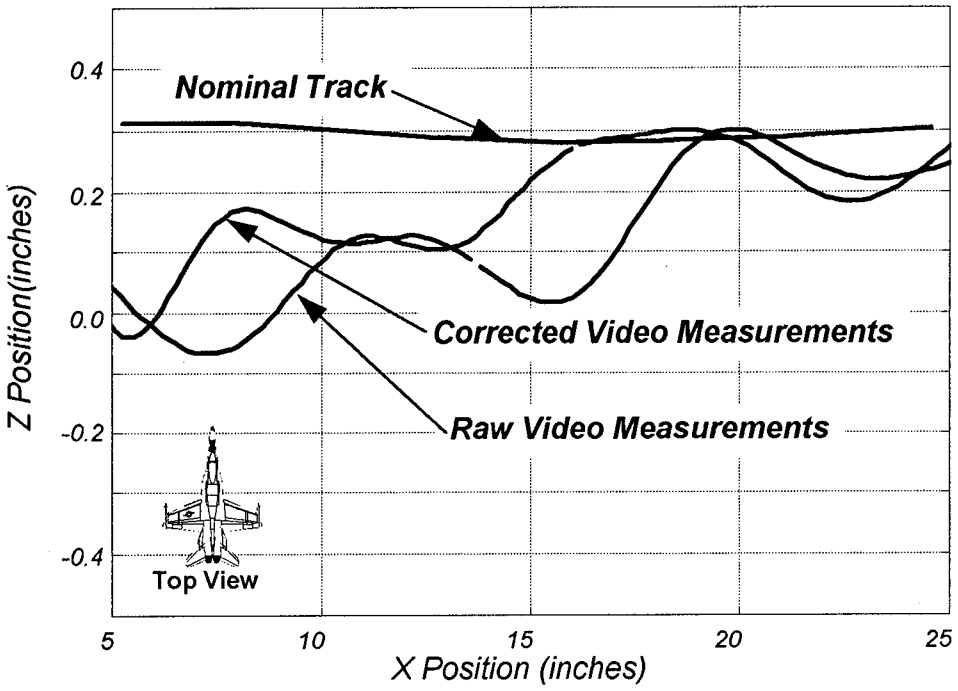

Fig. 27 Moving Cameras - Trajectory out of Plane.

The same numerical differentiator is used on the corrected trajectories to derive the velocity over the path. The velocities provided by the EV system are in the same range as those calculated by observing the target passing the fixed markers (Fig. 28). The biggest difference between the results obtained from the stationary and moving cameras is a 0.25 ft/sec decrease in precision. This change is seen graphically by the increase in the sinusoidal nature of Fig. 28 compared with the relatively flat curve for the stationary results on page 32. This change is a direct result of combining the uncertainty of two fixed markers with that of the moving target. Then

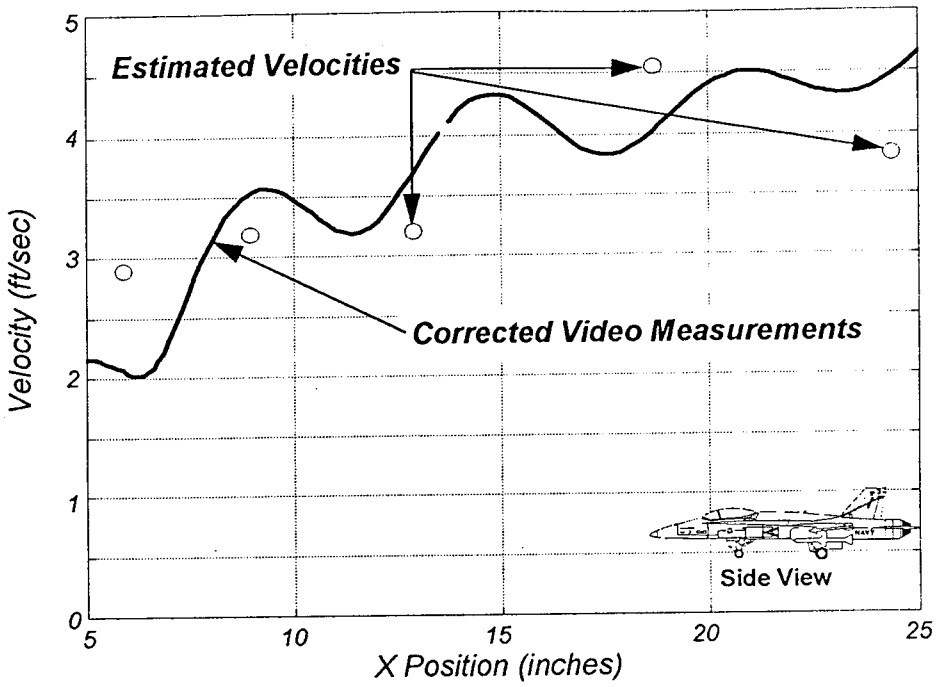

Fig. 30 Moving Cameras - Horizontal Velocity.

Ideally the trolley moves parallel to the X axis, so there should be no vertical velocity. Fig. 31 shows that camera motion "created" an artificial vertical velocity. After the trajectory was corrected for the camera motion, the vertical velocity was nearly reduced to zero. The average error for vertical velocity with camera motion was 0.007 ft/sec, compared with 0.002 ft/sec for stationary cameras (See page 34). The standard deviation also went up from 0.040 ft/sec up to 0.103 ft/sec. This indicates that both accuracy and precision are affected with camera motion.

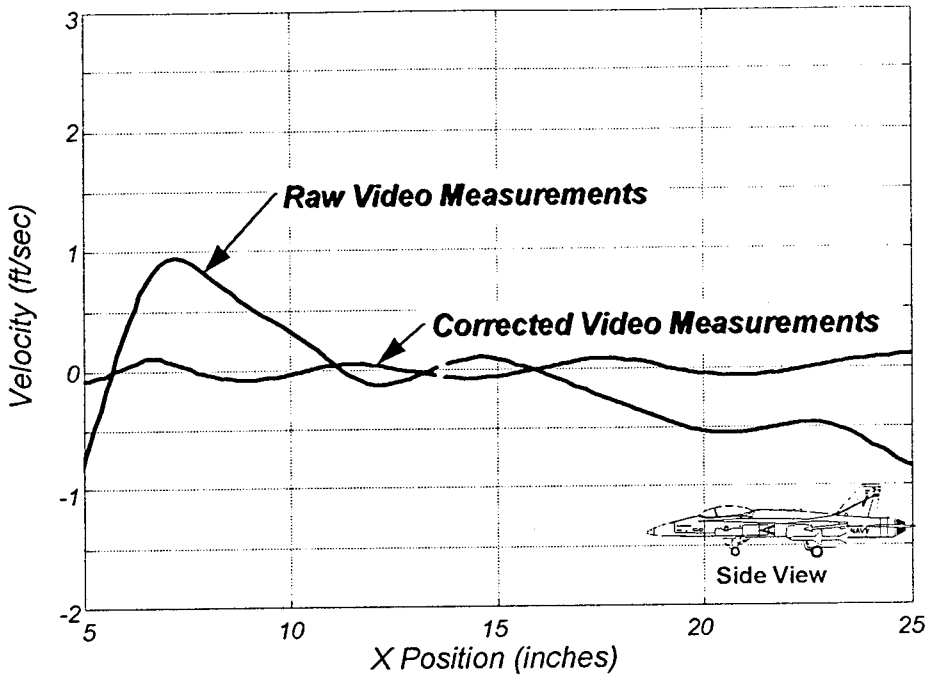

Fig. 31 Moving Cameras - Vertical Velocity.

The out of plane velocity with the cameras moving follows the same trend as with the stationary cameras (Fig. 32). The lack of stereo depth perception causes the uncertainty to be roughly an order of magnitude greater than for the values in the XY plane with combined translational and rotational camera movement. The maximum error of 0.5 ft/sec is the same in this case as in the stationary camera results on page 35. The average error increases with camera motion from 0.045 ft/sec to 0.073 ft/sec. The standard deviation grows dramatically from 0.189 ft/sec to 0.587 ft/sec.

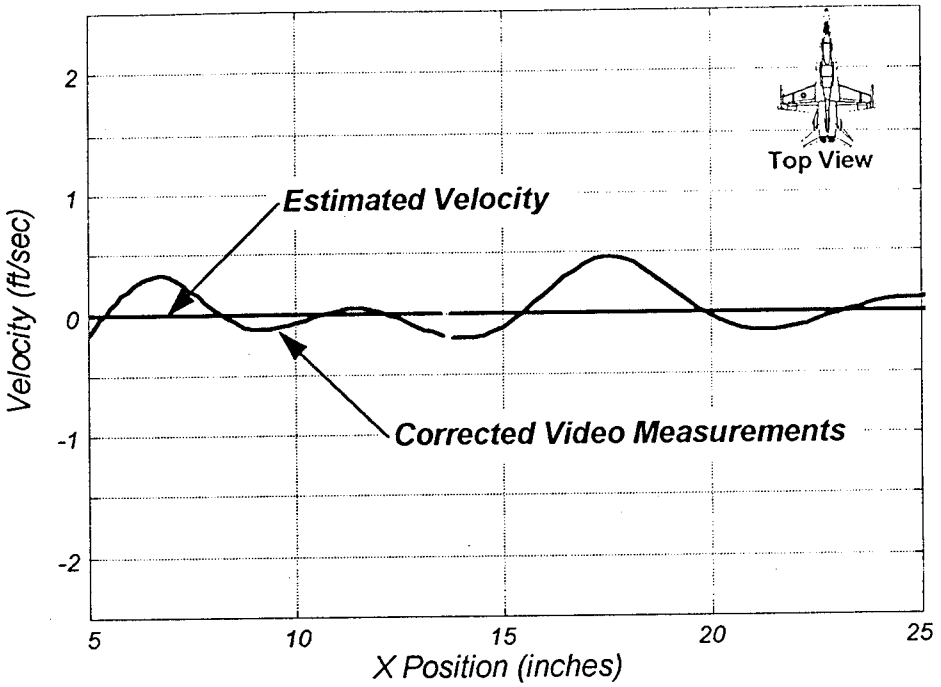

Fig. 32 Moving Cameras - Out of Plane Velocity.

The increase in the uncertainty of the trajectory propagated into the calculation of acceleration (Fig. 33), just like it did for the velocity estimates. All of the derived values depend on the accuracy of the trajectory data. The decrease in precision is also seen in the increased variation of acceleration along the trajectory. The 20 ft/sec^2 variation in acceleration is greater than that seen on page 33 for the stationary camera results. The added uncertainty with camera motion is amplified by the double numerical differentiation required to obtain acceleration.

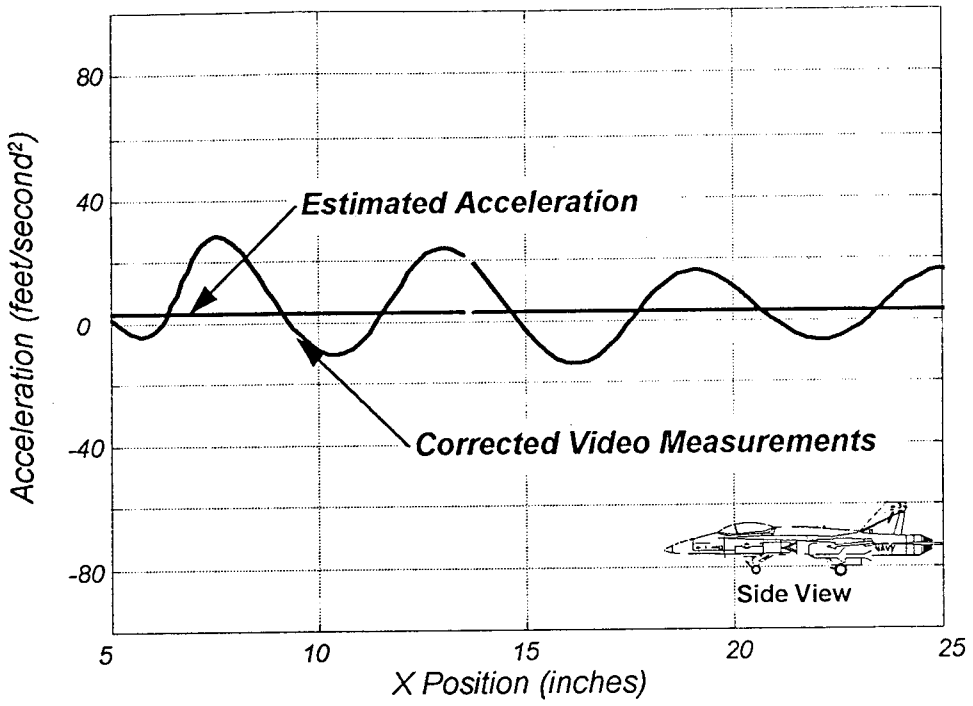

Fig. 33 Moving Cameras - Horizontal Acceleration.

Since the accuracy of the moving target depends on the accuracy of the fixed reference markers, especially when the cameras were in motion, the selection of a pair of control points is critical. To explore this idea, twelve combinations of different control points were examined to decide which pair provides the best trajectory.

Fig. 34 shows the control points used as references for the camera motion have a dramatic influence on the results. It seems obvious that points in the primary focus region should produce better results. However, this assumption was not true. Both points 6 and 7 are in the primary focus region, but performed poorly when applied as references for correcting camera motion. The best pairs are ones that span

the region of best focus with the larger distances between them. This pointed out that the distance between the two points is even more important than just points interior to the focus region.

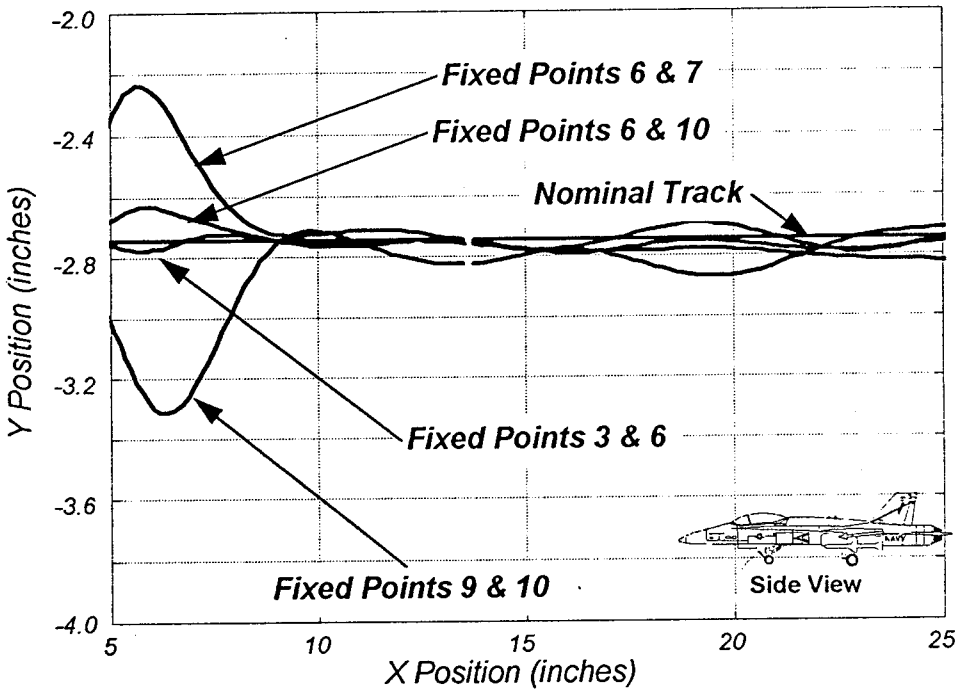

Fig. 34 Moving Camera - Point Selection.

The sensitivity of the results to the selection of the control point pair is directly linked to how the relative motion algorithm in Appendix A corrects camera motion. If two points are close together, like points 6 and 7 or points 9 and 10, the uncertainty in their location contributes more dramatically to the uncertainty in computing the rotation angle needed. This idea is visualized by placing three coins in a row with the first two much closer together than the third (Fig. 35). If the last two coins are both moved down an inch to represent the uncertainty in their location, two

different rotation angles result. A much larger angle results from using coins 1 and 2, rather than using coins 2 and 3.

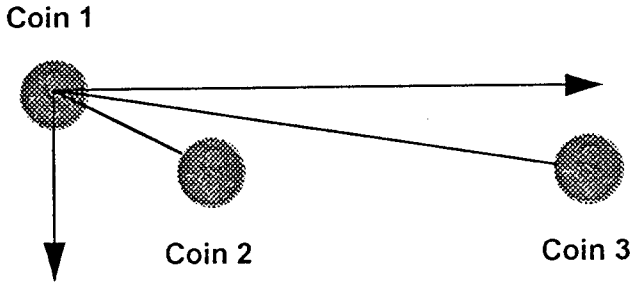

Fig. 35 Uncertainty in Computing Rotation.

This effect is also apparent because the uncertainty in the trajectory is largest at the beginning and at the end of the run. This principle can also be demonstrated with the same three coins. If the three coins are in a line and the last two are rotated through the same erroneous angle relative to coin 1, the last coin is displaced the most.

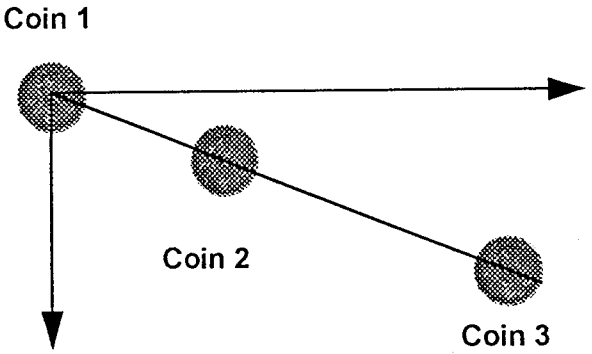

Fig. 36 Effect of Uncertainty in Rotation.

To help quantify the accuracy of the system, all of the relative errors of the fixed markers over a one second time interval (200 data points) were averaged together, and the standard deviation from the average calculated. These primitive statistical measures are also calculated for the simulated trajectory and vertical velocity of the target. The effect motion had on the accuracy and precision of the measurements is shown in Table 1. For all cases, the movement of the cameras increased the mean error, and lowered the precision of the measurement. The loss in depth perception is also apparent by the increase in mean error and standard deviation between the in plane and out of plane measurements.

Table 1 Comparison of Accuracy and Precision.

Type of Measurement	Stationary Cameras Mean Error	Moving Cameras Mean Error	Stationary Cameras Standard Deviation	Moving Cameras Standard Deviation
In Plane Fixed Point	0.020 (in.)	0.033 (in.)	0.017	0.066
Out of Plane Fixed Point	0.073 (in.)	0.099 (in.)	0.125	0.144
In Plane Trajectory	0.002 (in.)	0.009 (in.)	0.011	0.025
Out of Plane Trajectory	0.133 (in.)	0.153 (in.)	0.127	0.137
In Plane Velocity	0.002 (ft/sec)	0.007 (ft/sec)	0.040	0.103
Out of Plane Velocity	0.045 (ft/sec)	0.073 (ft/sec)	0.189	0.587

Full Scale Mockup Results

The ultimate test of system accuracy lies in how closely a smoke puff can be located on HARV itself. The last series of tests were aimed at answering this question with the equipment on hand. The actual cameras and lenses to be used for

the HARV flights were not available. The same Fairchild-Weston video cameras as before were used. The planned use of high speed motion picture cameras for the flight tests are designed to give higher frame rates, and picture resolution. The higher frame rate is useful during dynamic maneuvers since a higher number of data points is obtained per smoke packet. A higher frame rate also allows events with higher frequencies to be measured accurately. Generally, one needs to sample with an order of magnitude higher than the event being measured. Without these cameras, any errors in changing from high speed film to video tape, and any errors due to different lenses could not be evaluated.

The data collection and filtering techniques previously described were utilized for these test runs. All data were collected at the Texas A&M Flight Mechanics Laboratory hangar with the EV System.

The first area addressed is that of focus. Only about one third of the mockup could be in focus at one time with the available camera lenses. As in the small scale test, focus is a major factor and is shown in Fig. 37. The points in the focus region (1, 3, and 7) were all within one inch of their known locations. The fixed markers outside the region (10, 11, and 12) were uncertain by over a foot. The most notable difference from the small scale test was that the accuracy of the point out of plane was only slightly higher as those of points in plane. This result is likely due to the greater separation between cameras for the full scale test. This displacement gives the system a boost in stereo vision by increasing the relative angles between the two cameras. It should also be noted that the camera location for the small scale board

was based on filed of view, and therefore, the two test do note have identical geometry.

Fig. 37 also shows the transit uncertainty in locating the fixed markers. Each pair of transit sites produces a location for each target. Six sets of coordinates were averaged together to provided the nominal location, and the maximum difference between the sets became the uncertainty for measurement. This was approximately 1.1 inches.

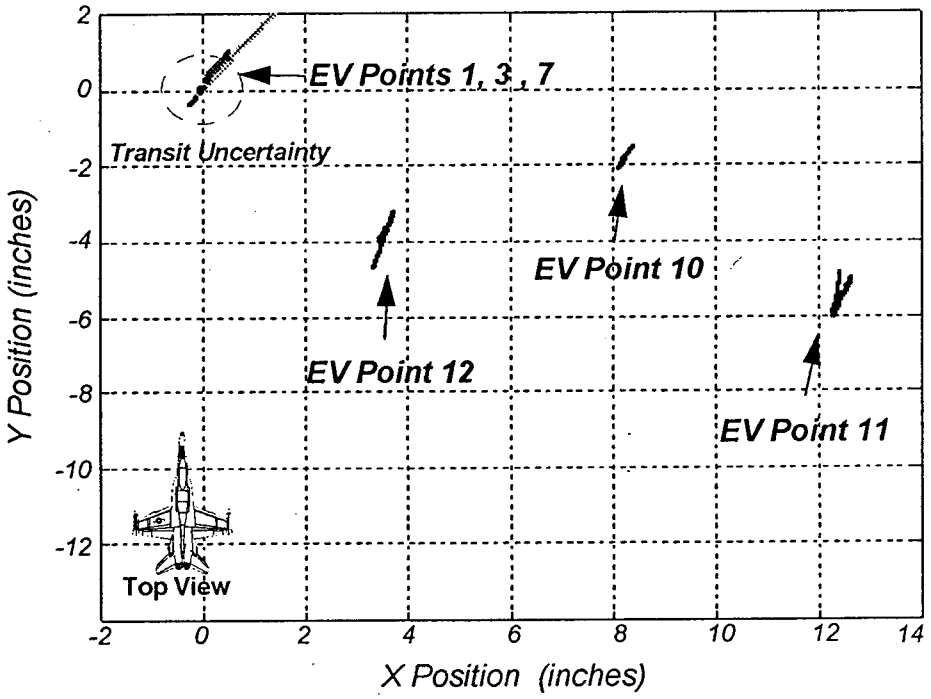

Fig. 37 Full Scale - Relative Errors.

The errors in elevation for various control points that were in the focus region are also within an inch. Some points out of focus, (10, 11, and 12) were over a foot in error for the run (Fig. 38). Both points 11 and 12 are close to each other on the

mockup, but have significantly different relative errors. This indicates that the degree of focus does not affect uncertainty linearly. This same result is seen in Fig. 27 on page 40. Being out of focus just means that the uncertainty grows for the measurement.

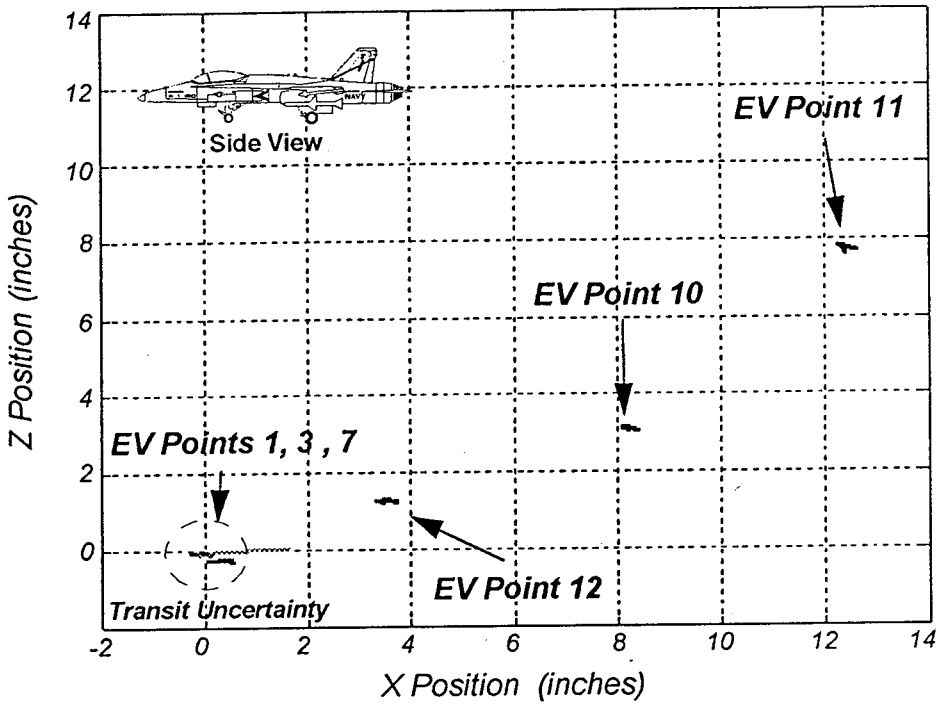

Fig. 38 Full Scale - Errors in Elevation.

The importance of focus was also evident by examining the accuracy of EV when the aft control points were in focus. The cameras for this run were not moved, only the focus was changed. This indicates that focus controls the majority of the system's uncertainty in this case. All of the relative errors were reduced to under one

inch like the forward control points in the first data run (Fig. 39). Notice that the scale is enlarged in Fig. 39.

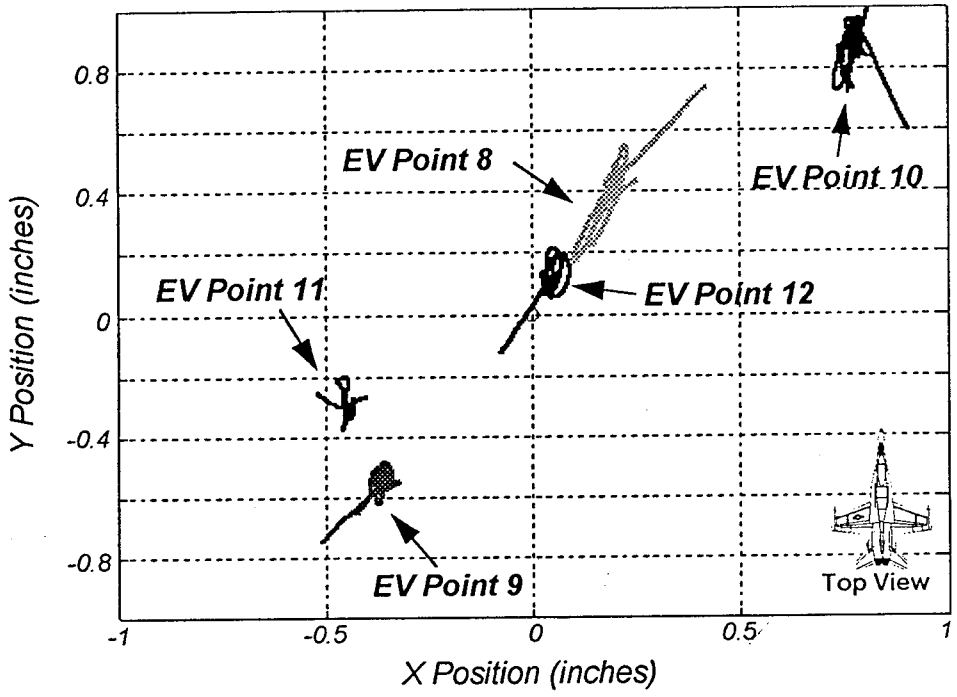

Fig. 39 Full Scale - Relative Error of Aft Control Points Focused.

The same holds true for the relative errors in elevation once the points were focused in (Fig. 40). It is also important to notice that once again there is no significant difference in determining the location of the point out of plane. This result is again contrary to the systems depth perception during the small scale runs. The only significant difference between the camera setups are the distances between them.

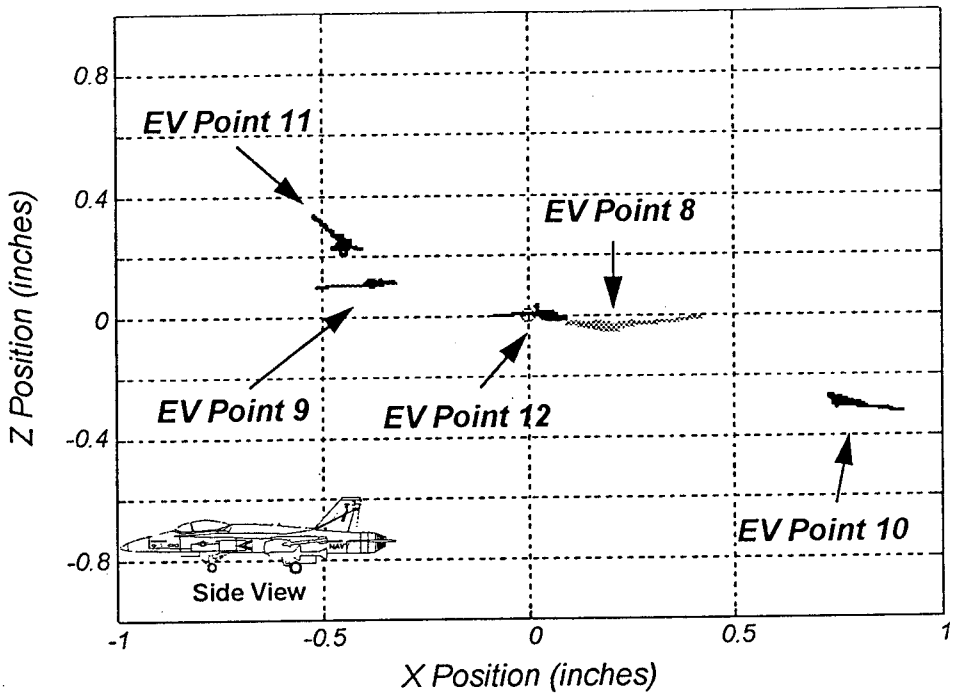

Fig. 40 Full Scale - Elevation Error of Aft Points Focused.

NASA's major concern with the system's accuracy after reviewing the small scale results, is the reduction in accuracy for out of plane movement with the cameras located on the wing tip. This loss of accuracy reduces the ability to track the movement of the vortex toward the cameras. This concern is the main reason that the moving target traces a circular trajectory toward the cameras. With the target track in a focused region of the field of view, the system tracks the sphere within 1.5 inches of the actual path (Fig. 41). The average error in location for the circular trajectory is 0.98 inches with a standard deviation of 0.35 inches.

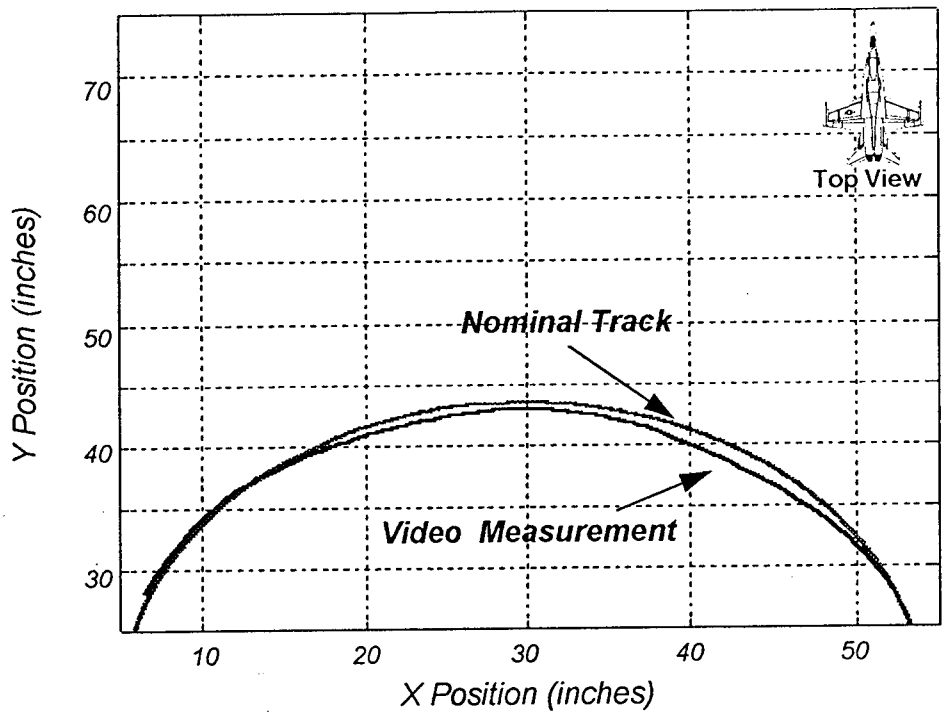

Fig. 41 Full Scale - Trajectory of Target.

With an accurate trajectory, velocity is determined using the same Lagrangian differentiator described on page 31. All values of velocity are within 2 ft/sec (Fig. 42). The mean error in velocity is 0.77 ft/sec with a standard deviation of 1.7 ft/sec. The high standard deviation results from the fact that over one frame, the target travels less than one inch, but the system's location for the point may be in error up to an inch. This "creates" false changes in velocity. The estimated velocity is based off the assumption that the motor speed remains constant. The ability to determine an accurate velocity is also set by the frame rate and target speed. If the frequency of

the target's motion is equal to the sample rate of the camera, the target appears to be motionless to the system.

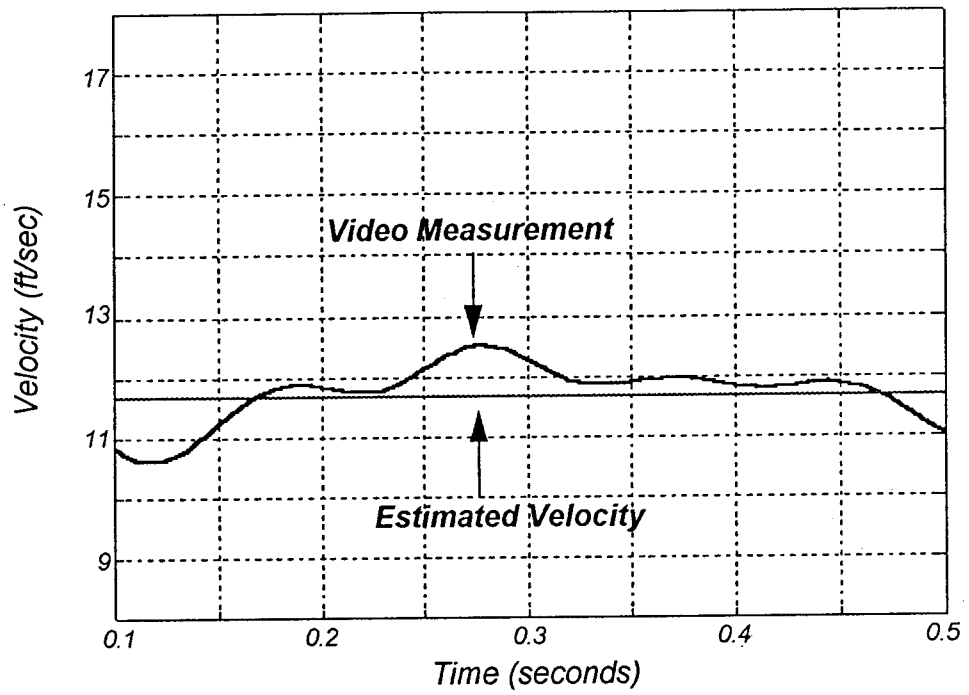

Fig. 42 Full Scale - Target Velocity.

Table 2 compares the changes in accuracy and precision with increasing velocity over a 0.5 second time period (100 points per target). There is both an decrease in accuracy and precision as the velocity of the target increases. The standard deviation is almost double for the fastest target when compared to the slowest tested. The use of high speed film cameras for the actual flight tests may help to alleviate this problem, but further testing with frame rates must be accomplished to answer this question.

Table 2 Velocity Comparison.

Velocity	Mean Error	Standard Deviation
4.25 (ft/sec)	0.2471 (ft/sec)	1.076
8.55 (ft/sec)	0.2765 (ft/sec)	1.1931
11.65 (ft/sec)	0.7746 (ft/sec)	1.708
16.25 (ft/sec)	0.6821 (ft/sec)	1.913

The acceleration for the target is assumed to be zero since a constant speed motor is used to estimate a constant velocity. The results, however, show some variation in the acceleration (Fig. 43). The average acceleration is 3.5 ft/sec^2 with a standard deviation of 27.3 ft/sec^2. The increase in uncertainty and the decrease in precision between the velocity and acceleration data is a result of the added information lost with the additional differention required for acceleration.

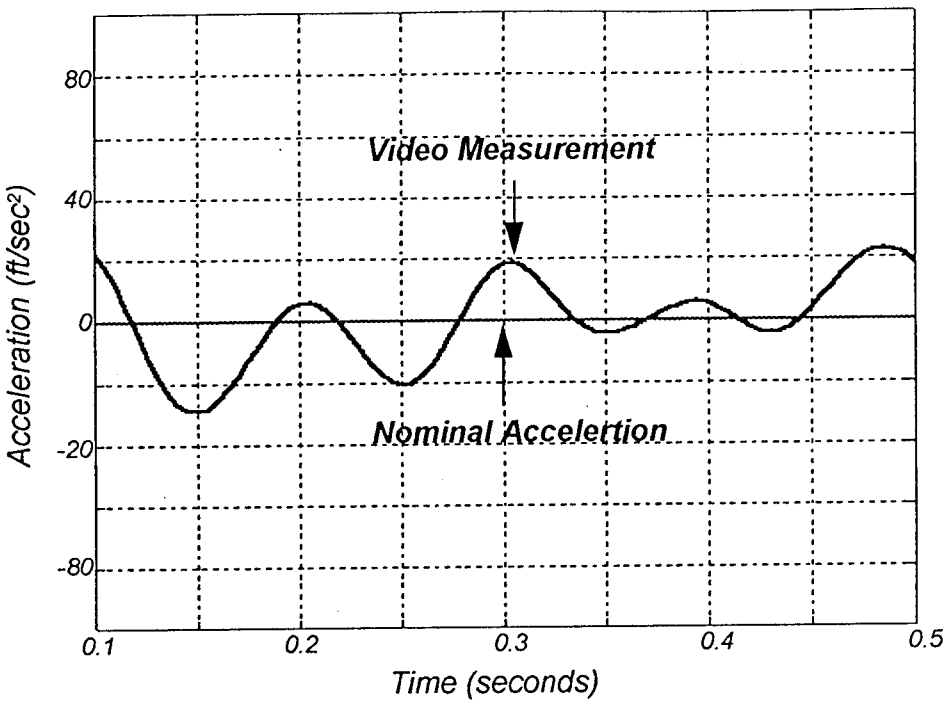

Fig. 43 Full Scale - Target Acceleration.

The relative errors from the fixed points that were in focus were averaged together to find the mean error and standard deviation for the full scale model. Table 3 shows that the system estimates elevation better than X of Y. There is a slight decrease in accuracy and precision for out of plane measurements (Y axis). This difference, however, is not as severe as in the small scale tests, and does prevent relevant data from being collected of flight tests. This is due to the greater distance between the cameras, which increases the relative angles to a target. The accuracy of velocity is much higher than that for acceleration. This is due to the information lost during the double integration required for acceleration. The position data are based

off of a one second period (200 points per location), while velocity and acceleration are for 0.5 seconds (100 points per target).

Table 3: Error and Standard Deviation.

Axis	Mean Error	Standard Deviation
X	0.4878 (in.)	0.1972
Y	0.7982 (in.)	0.2806
Z	0.3197 (in.)	0.0912
Velocity	0.568 (ft/sec)	1.708
Acceleration	3.508 (ft/sec2)	27.25

Comparisons Between the Tests

It is important compare the results between the full scale mockup and the small scale lab board, in order to predict what might be expected on actual HARV flights. During this comparison it must be kept in mind that only general trends are valid because of different fields of view, lighting, target trajectories, and target sizes.

First, camera motion increases the uncertainty for the trajectory because several points are needed to correct for the motion. Table 1 on page 50 shows that the error in locating a non moving target increased 1.5 times with camera motion. This majority of this increase originates from the relative motion algorithm since three locations must be known instead of just one.

The accuracy in predicting a velocity is dependent upon the accuracy of the trajectory, but on the ratio between the translational velocity of the vortex and the frame rate for the cameras.

To develop a better sense as to the type of accuracy one cane expect with video imaging, the relative errors for the small and full scale tests were normalized by the length of their field of view (Table 4). The field of view for the small scale test board is three feet, while the filed of view for the full scale mockup is 23 feet. These values will also change with the quality of lens calibration, focus region, and camera location calibration, but similar results should be achievable for any size test object.

Table 4 Normalized Percent Error.

TEST	Percent Error
Lab Test Board	0.53%
Full Scale Mockup	0.65%

CONCLUSIONS AND RECOMMENDATIONS

Conclusions

The major objectives of this study are to produce a method of eliminating camera motion from data collected using the ExpertVision system and to estimate this system's accuracy in locating vortices on the F/A-18 HARV.

The utilization of a simple relative motion algorithm allowed for the error created by camera motion to be effectively eliminated from the targets trajectory. The relative uncertainty in the location of the target did increase due to the employment of two fixed control points. The algorithm is effective in reducing both the apparent translation from wing bending and the rotation caused by wing torsion.

The accuracy of the corrected path is affected not only by the accuracy of the predicted location of the fixed points, but by their location with respect to each other. Control points that were close together gave larger uncertainties in the rotation. These uncertainties propagated to the moving target during the correction. By selecting points across the field of view this uncertainty is minimized.

The requirement to measure three points accurately did corrupt the velocity and acceleration data, however. Both rely heavily on the accuracy and precision of the targets of interest at any give instant. Numerical differentiation does not help since it is an information losing process.

The use of MATLAB for post processing trajectory data is very useful. The Signal Processing Tool Box allows a cutoff frequency to be determined and a 4th order Butterworth filter to be constructed. The data are filtered forwards and backwards. The use of this software allows for built in matrix manipulation and math functions to be applied to the data. EV, on the other hand, contains few built in

functions, and requires the user to write additional functions. Also, using EV for data file manipulation requires the user to work with a set file format.

The accuracy of the EV system is most profoundly affected by camera location and focus. The location affected mainly depth perception, while focus significantly increased error in every direction. The full scale mockup results suggest that the system has an accuracy of about one inch for full scale aircraft dimensions. If the added error factor in correcting for camera motion remains the same on the HARV, then the vortex should be located within 1.5 inches of its actual position on average.

During small scale tests, the camera location increased the relative error in determining trajectory motion toward the cameras by an order of magnitude. This problem did not occur in the full scale tests due to the added separation of the cameras. For the full scale tests, the target moved in a circular arc toward the cameras and the system accurately measured its position.

Focus has the biggest influence on the performance of the system, both in the lab and at full scale dimensions. Measurements could be as much as a foot in error during the full scale tests if the control points were not carefully focused.

Camera location and lighting dictate system precision. These factors must be emphasized when using this type of measurement scheme on a test vehicle in flight.

By normalizing the relative errors by the field of view, the EV system provided the location of points within less than 1% of the length of the field of view for two cameras. The error for the small test board was 0.53%, and the full scale mockup was 0.65% the total length of the test region.

All validation tests so far indicate that ExpertVision offers the flight test community a useful, nonintrusive measurement tool. It will return quantified data

about the vortical flow field on a test aircraft if a suitable smoke visualization, and two cameras are carefully calibrated and located on the airframe.

Recommendations

The only way to completely validate the use of ExpertVision for tracking vortical flow on a test aircraft is to do it. The high speed cameras should be mounted on the HARV for the forebody vortex control tests. The flight tests need to examine tracking the vortex core and estimate system accuracy. Three fixed markers would provide the necessary data to determine the accuracy. Two of the fixed points would be used to correct the relative motion of the third. The result should be a stationary target at its known location.

Actual test flights would also help to build a better knowledge base on using the natural lighting to provide the best contrast for EV data collection. Lighting changes can not be adequately simulated on the ground. More experience would also be gained in isolating the leading edge of each smoke packet and how diffusion of the smoke might alter the results.

Before flight tests are conducted each camera lens must be calibrated to compensate for any error in the optics. This effort might also look into correcting the focus problem, by using a numerical correction to the data during post processing. The conversion from the high speed film to video format must also be investigated.

In the area of better understanding video imaging, more work needs to be done in determining the factors that affect accuracy. Tests must be conducted to determine how frame rate and target velocity affect the system's performance in estimating velocity and acceleration. It would be beneficial to have an a priori knowledge of system accuracy without having to create full scale mockups.

The final recommendation is in the area of customizing a digital filter for the test. A custom filter must be developed to increase the precision of the data collection, and gain a better understanding of how filter employment affects the data.

REFERENCES

[1]Hall, R.M., Banks, D.W., Fisher, D.F., Ghaffari, F., Murri, D.G., and Ross, J.C., "A Status Report on High Alpha Technology Program (HATP) Ground Test to Flight Comparisons," NASA-CP10143, Vol. 1, *NASA High Angle-of-Attack Conference*, Edwards AFB, CA., July 1994.

[2]Fisher, D.F., and Lanser, W.R., "Flight and Full-Scale Wind-Tunnel Comparison of Pressure Distributions from an F-18 Aircraft at High Angles of Attack," NASA-CP10143, Vol. 1, *NASA High Angle-of-Attack Conference*, Edwards AFB, CA., July 1994.

[3]Murman, S.M., and Rizk, Y.M., "Numerical Simulation of the Flow about an F-18 Aircraft in the High-Alpha Regime," NASA-CP10143, Vol. 1, *NASA High Angle-of-Attack Conference*, Edwards AFB, CA., July 1994.

[4]Biedron, R.T., and Whitaker, D.L., "Hybrid Structured/ Unstructured Grid Computations for the F/A-18 at High Angle of Attack," NASA-CP10143, Vol. 1, *NASA High Angle-of-Attack Conference*, Edwards AFB, CA., July 1994.

[5]Bowers, A.B., Regenie, V.A., and Flick, B.C., "F-18 High Alpha Research Vehicle: Lessons Learned," NASA-CP10143, Vol. 2, *NASA High Angle-of-Attack Conference*, Edwards AFB, CA., July 1994.

[6]Meyn, L.A., "Full Scale Wind Tunnel Tests of an F/A-18," NASA-CP-3137, Vol. 3, *NASA High Angle-of-Attack Conference,* Edwards AFB, CA., April 1992, pp. 199-222.

[7]Fisher, D.F., Banks, D.W., and Richwine, D.M., "Surface Flow Visualization of Separated Flows on the Forebody of an F-18 Aircraft and Wind-Tunnel Model," TM-100436, NASA, Edwards AFB, CA., June 1988.

[8]Fisher, D.F., Banks, D.W., and Richwine, D.M., "F-18 High Alpha Research Vehicle Surface Pressures: Initial In-Flight Results and Correlation with Flow Visualization and Wind-Tunnel Data," TM-101724, NASA, Edwards AFB, CA., August 1991.

[9]Fisher, D.F., Del Frate, J.H., and Zuniga, F.A., "Summary of In-Flight Flow Visualization Obtained from the NASA High Alpha Research Vehicle," TM -101743, NASA, Edwards AFB, CA., January 1991.

[10]Williams, D.L., and Nelson, R.C., "Free-to-Roll Test of the X-31 and F-18 Subscale Models with Correlation to Flight Test Results," NASA-CP10143, Vol. 1, *NASA High Angle-of-Attack Conference*, Edwards AFB, CA., July 1994.

[11]Meryn, L.A., James, K.D., and Geene, R.J., "Correlation of F/A-18 Tail Buffet Results," NASA-CP10143, Vol. 1, *NASA High Angle-of-Attack Conference*, Edwards AFB, CA., July 1994.

[12]Canter, D., "X-31 Post-Stall Envelope Expansion and Tactical Utility Testing," NASA-CP10143, Vol. 2, *NASA High Angle-of-Attack Conference*, Edwards AFB, CA., July 1994.

[13]Anna, P.D., and Kidman, D.S., "Flight Test Results of the F-16 Aircraft Modified with the Axisymmetric Vectoring Exhaust Nozzle," NASA-CP10143, Vol. 2, *NASA High Angle-of-Attack Conference*, Edwards AFB, CA., July 1994.

[14]Huber, P., and Schellenger, H., "X-31 Quasi-Tailless Flight Demonstration," NASA-CP10143, Vol. 2, *NASA High Angle-of-Attack Conference*, Edwards AFB, CA., July 1994.

[15]Walchli, L.A., "Flight Evaluation of Pneumatic Forebody Vortex Control in Post-Stall Flight," NASA-CP10143, Vol. 3, *NASA High Angle-of-Attack Conference*, Edwards AFB, CA., July 1994.

[16]Ralston, J., "Examination of Vortex Control on a Chined Forebody During Maneuvering Flight Conditions," NASA-CP10143, Vol. 3, *NASA High Angle-of-Attack Conference*, Edwards AFB, CA., July 1994.

[17]Boalbey, R.E., Citurs, K.D., and Wayne, L.E., "Integration of a Mechanical Forebody Vortex Control System into the F-15," NASA-CP10143, Vol. 3, *NASA High Angle-of-Attack Conference*, Edwards AFB, CA., July 1994.

[18]Murri, D.G., Shah, G.H., and DiCarlo, D.J., "Preparations for Flight Research to Evaluate Actuated Forebody Strakes on the F-18 High-Alpha-Research Vehicle," NASA-CP10143, Vol. 3, *NASA High Angle-of-Attack Conference*, Edwards AFB, CA., July 1994.

[19]"ExpertVision User's Manual", Motion Analysis Corp., Santa Rosa, CA., 1989.

[20]Ward, D.T., and Myatt, J.H., "Preliminary Design of an Intermittent Smoke Flow Visualization System," CR-186027, NASA, Edwards AFB, CA., June 1993.

[21]Ward, D.T., and Dorsett, K.M., "Flight Validation of a Pulsed Smoke Flow Visualization System," CR-186026, NASA, Edwards AFB, CA., September 1993.

[22]Freudinger, L.C., "Flutter Clearance of the F-18 High-Angle-of-Attack Research Vehicle with Experimental Wingtip Instrumentation Pods," TM- 4148, NASA, Edwards AFB, CA., October 1989.

[23] "MATLAB User's Manual," The Math Works Inc., South Natick, MA., 1989.

[24]Brinker, R.C., and Wolf, P.R., *Elementary Surveying*, Harper and Row, New York, 1984.

APPENDIX A

RELATIVE MOTION MATLAB M-FILE

```
function [xcrt,ycrt] = vrela(x1, y1, x2, y2, xt, yt, xact1, yact1, xact2, yact2)

% This M file corrects for motion of EV cameras using two fixed
% reference markers and the target of interest
% [xcrt,ycrt] = vinrela(x1, y1, x2, y2, xt, yt, xact1, yact1, xact2, yact2)
% x1, y1 are the coordinates from the trajectory of the first fixed point
% x2, y2 are the coordinates from the trajectory of the second fixed point
% xt, yt are the coordinates of the targets trajectory
% xact1, yact1 are the actual coordinates for the first fixed marker
% xact2, yact2 are the actual coordinates for the second fixed marker

% First calculate the relative angle between the two fixed points
% in the non moving frame of reference

dxfix = xact2 - xact1;
dyfix = yact2 - yact1;
fixang = atan(dyfix./dxfix);

% Next calculate actual angle between the two reference points in the
% moving frame

dxmv = x2 - x1;
dymv = y2 - y1;
angmv = atan(dymv./dxmv);
delang = angmv - fixang;

% Calculate the angle between the first fixed point and the moving target
% and correct it for the delta angle of rotation

dxtrgt = xt-x1;
dytrgt = yt-y1;
tang = atan(dytrgt./dxtrgt);
% third quadrant check
[n,m] = size(x1);

for i = 1:n
 if (dxtrgt(i) < 0.0)
  if (dytrgt(i) < 0.0)
```

```
   tang(i) = atan(dytrgt(i)./dxtrgt(i)) + pi;
  end
 end
end

% second quadrant check

for j = 1:n
 if (dxtrgt(j) < 0.0)
  if (dytrgt(j) > 0.0)
   tang(j) = atan(dytrgt(j)./dxtrgt(j)) + pi;
  end
 end
end

corang = tang - delang;
trgtrang = sqrt(dxtrgt.^2 + dytrgt.^2);
dxcrt = trgtrang .* cos(corang);
dycrt = trgtrang .* sin(corang);



% Translate the corrected values of the target position from the fixed
% reference coordinates to that of the system

xcrt = dxcrt + xact1;
ycrt = dycrt + yact1;

% end of program
```

APPENDIX B

MATLAB MAT FILES FROM TEST RUNS

The following MATLAB .MAT files provide time history data for each control point and target for various runs of the small scale board and the full scale mockup. The actual files are located on the 3.5 inch floppy disk provided with this document. The time history for each control point is contained inside a matrix with the control point number added on to the end of the file name. A "t" at the end matrix designates the time history for the target. Each matrix contains three columns representing the X, Y, and Z coordinates. The files included are:

Small Scale Runs

ss3j1.mat	Stationary Cameras, 2 ft/sec Target
ss3j2.mat	Stationary Cameras, 4 ft/sec Target
sp3j1.mat	Simulated Wing Bending, 2 ft/sec Target
sp3j2.mat	Simulated Wing Bending, 4 ft/sec Target
st3j1.mat	Simulated Wing Torsion, 2 ft/sec Target
st3j1.mat	Simulated Wing Torsion, 4 ft/sec Target
sf3j1.mat	Simulated Full Motion, 2 ft/sec Target
sf3j2.mat	Simulated Full Motion, 4 ft/sec Target

Full Scale Mockup

mocal1.mat	Stationary Cameras, 4 ft/sec Target
mocal2.mat	Stationary Cameras, 8 ft/sec Target
mocal3.mat	Stationary Cameras, 12 ft/sec Target
mocal4.mat	Stationary Cameras, 16 ft/sec Target
mocal5.mat	Stationary Cameras, Aft Control Points in Focus

VITA

Vincent Joseph Sei was born December 30, 1969, in Albuquerque New Mexico. He graduated from the United States Air Force Academy in 1993 with a Bachelor of Science Degree in Aeronautical Engineering, and a Commission in the United States Air Force. He is now assigned to the F-15 Combined Test Force at Edward's Air Force Base California. He can be reached at 817 Parkland Cr. S.E., Albuquerque, New Mexico, 87108.